# SUPERSONIC LAMINAR BOUNDARY LAYER SEPARATION NEAR A COMPRESSION CORNER

by

A. A. Sfeir



REPORT NO. AS-69-6
AFOSR GRANT 268-68
March 1969

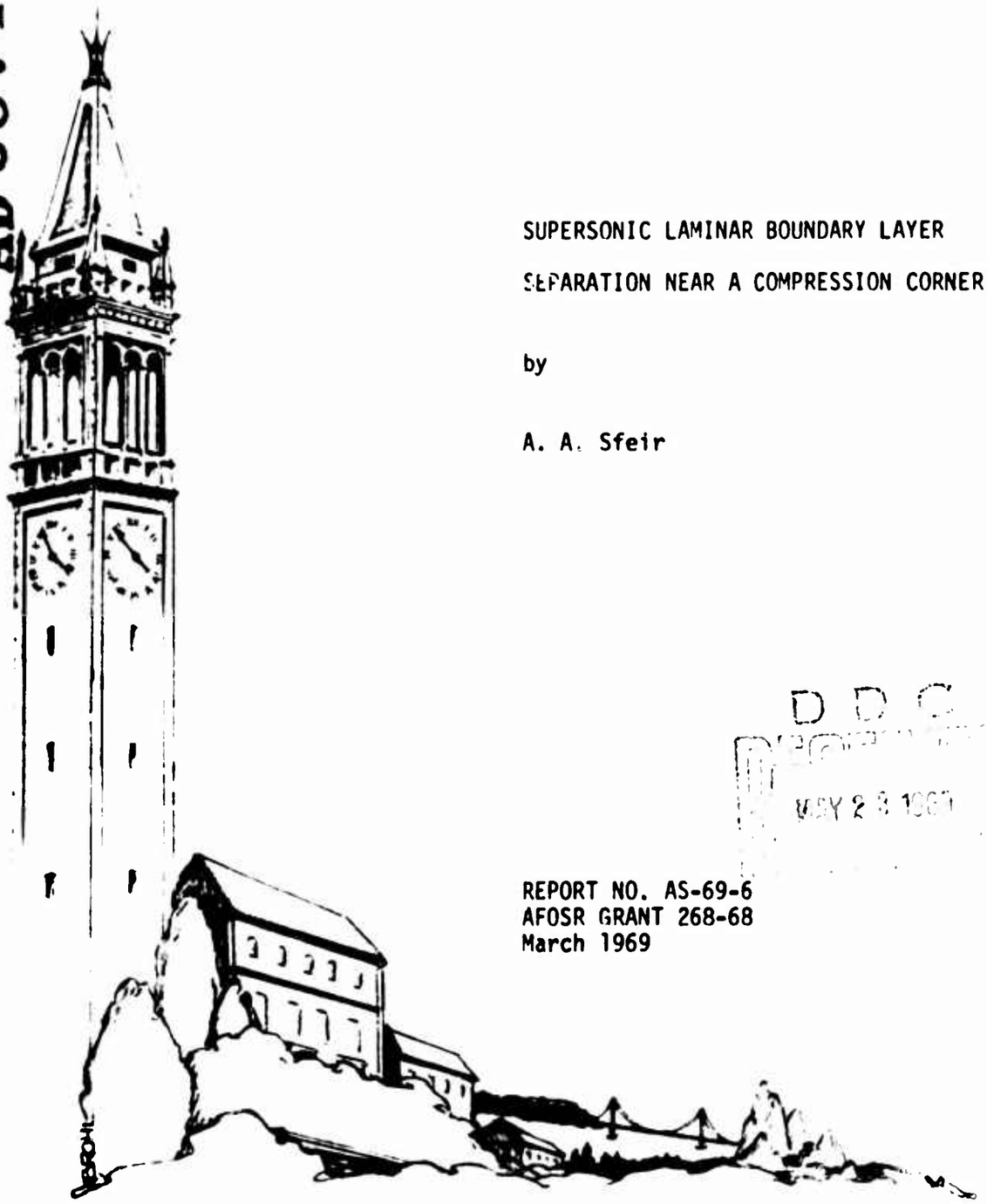

**COLLEGE OF ENGINEERING**

**UNIVERSITY OF CALIFORNIA, Berkeley**

AFOSR GRANT 268-68
REPORT NO. AS-69-6
MARCH 1969

SPONSORED BY
THE AIR FORCE
OFFICE OF SCIENTIFIC RESEARCH

# SUPERSONIC LAMINAR BOUNDARY LAYER SEPARATION NEAR A COMPRESSION CORNER

A. A. Sfeir

Submitted in partial satisfaction of the requirements
for the degree of Doctor of Philosophy in Engineering



March 1969

University of California
Aeronautical Sciences Division
Berkeley, California 94720

## ABSTRACT

Detailed measurements were performed in the region of interaction of a laminar boundary layer with a compression corner at Mach numbers near 2.5. Different models were tested permitting variation in the angle of compression and the conditions downstream of reattachment.

The heat flux and the resistance of equilibrium of a hot wire anemometer at any location in the flow field were measured. These measurements were supplemented by either the wall or the pitot pressure to compute all thermodynamic and dynamic variables.

The results permitted verification of the hypothesis of zero normal pressure gradients when the compression angle is small and the boundary layer is laminar. The enthalpy in the separated bubble was constant and equal to the wall enthalpy of a flat plate with attached laminar boundary layer at the same Mach number. Evidence of a reversed flow with velocities approximately 5% of the free stream velocity was observed. The recompression along the separating streamline was found to be very nearly isentropic. Critical points were located in the reattachment region and a physical explanation proposed with special emphasis on the location of transition.

TABLE OF CONTENTS

## LIST OF SYMBOLS

| | |
|---|---|
| AR | Aspect ratio $s/\ell$ |
| $C_1$, $C_2$ | Critical points |
| $C_R$, $C_N$ | Hot wire correction factors |
| d | wire diameter |
| h | enthalpy |
| i | current through the wire |
| Kn | Knudsen number |
| k | thermal conductivity |
| $\ell$ | length of flat plate ahead of compression corner |
| M | Mach number |
| Nu | Nusselt number |
| Pr | Prandtl number |
| p | pressure |
| q | total velocity |
| R | reattachment point |
| Re | Reynolds number |
| r | hot wire resistance |
| S | separation point |
| s | span of models |
| T | temperature |
| u | velocity in x direction |
| v | velocity in y direction |

$\alpha$ compression angle

$\delta_1$ boundary layer thickness

$\delta_2$ displacement thickness

$\delta_3$ momentum thickness

$\eta$ recovery ratio

$\rho$ density

$\mu$ viscosity

Frequently used subscripts

t total (temperature or pressure)

e equilibrium condition (adiabatic wire)

' conditions in free stream outside the boundary layer

f free molecular condition

c continuum condition

o condition in free stream ahead of interaction

## LIST OF FIGURE TITLES

## 1.0 INTRODUCTION

For the design of present day high speed aircraft it is becoming increasingly important to understand the behavior of supersonic boundary layers when exposed to sudden changes in free stream conditions. These changes could be caused, for example, by a shock impinging on the boundary layer or by a rapid change in the body shape. Experience has shown that even though the region where the viscosity acts is very thin, under certain flow conditions this layer can move away from the body, creating large shifts of the aerodynamic loads. It is, therefore, important to be able to predict these flow conditions and their effects on the boundary layer.

This type of phenomenon occurs on wings with trailing edges of finite thickness, causing an additional drag (base drag); it also occurs on reentry vehicles with flares, introducing a favorable effect on the aerodynamic heating. The type of flow investigated in this paper is the separation of a boundary layer caused by a sudden compression such as that on wings with flaps or ailerons, or the conical flare which follows the cylindrical section of a Gemini capsule. These flows all belong to a class of problems called separated flows. The problem which interests us is one of the most difficult, for, as will be seen later, neither the point of separation nor that of reattachment is fixed.

The physical features of the flow are as follows. A supersonic stream flowing past a flat plate is suddenly turned through a corner at a certain point $0$ (see Fig. 1). If the effects of viscosity are neglected the problem is a trivial one. A shock originating at $0$ will turn the stream through the deflection angle $\alpha$. If, however, viscosity is taken into account we know that there exists a thin layer near the wall which is

slowed down by friction. The bottom part of this layer will be subsonic, hence a shock cannot exist there. The pressure jump will be spread over a finite length. When this layer approaches the corner it will sense the pressure increase before reaching O. If the momentum of the particles in the boundary layer is not sufficiently large to overcome this unfavorable pressure increase the particles will move away from the wall. There then exists on the wall a stagnation point (S), which is called the separation point. A streamline (SA) originates from this point. As the flow separates the particles will pick up sufficient momentum to bring them into contact with the body at a point R, which is called the reattachment point. This point is also a stagnation point, and a streamline A'R terminates there. Using simple arguments based on conservation of mass we see that, provided no flow crosses the solid boundary between S and R, the streamline originating in S is the same one that terminates at R. Hence there exists a closed region SAA'RO which always consists of the same particles. Looking closely at this region we see that the forces acting on the particles within it are: shear stresses on the interface SR, and wall friction on SRO. The particles near SR will be moving downstream, so that other particles will have to replace them. This region therefore has a clockwise circulating motion. Actually, it is not correct to call the line SR an interface, because *a priori* no discontinuities of any sort occur on this line; it is merely the line that separates the particles which have sufficient momentum to overcome the pressure rise at the reattachment region from those which have insufficient momentum to overcome the pressure rise and are turned back into the region SRO; for this reason SR is called the separating streamline. The above simple arguments give a good picture of the

expected flow; howe , the difficulty lies in determining the locations of S and R, in being able to predict this location, in finding SR, and more generally, in being able to predict what will happen under a given set of conditions.

Theoretically, the difficulties appear quite discouraging at first glance. The principal difficulty is that the boundary layer equations are not expected to hold at the point of separation, since a normal pressure gradient may exist there. Even by assuming that there is in fact no appreciable normal pressure gradient it is still impossible to solve these equations because the streamwise pressure distribution is one of the unknowns. However, a great contribution has been made in this regard by Chapman, et al.,[1] who suggested a way to overcome this difficulty by assuming that the pressure distribution is conditioned by the interaction between the laminar boundary layer and the supersonic free stream. This assumption is justified by several experiments and is now widely used. It is called the "free interaction hypothesis." More precisely, this hypothesis implies that the interaction between the viscous layer and the supersonic free stream depends solely on local quantities and is not directly dependent upon the geometry which induces separation. An extension of this assumption for the nonadiabatic wall has been proved by Curle.[2]

Several theoretical solutions were found by using this simplification. An approximate solution based on the application of Howarth's transformation to the compressible boundary layer equations has been found by Curle. Other approximate methods based on consideration of the boundary layer as two layers, an inner layer in which viscosity and pressure forces are dominant, and an outer layer with inertia forces,

were also found by Gadd,[3] and Hakkinen, et al.[4] More sophisticated mathematical methods were used by Holt[5] and Lees and Reeves.[6] Holt uses a multi-moment method instead of edge boundary conditions as in Pohlhausen's method and expresses the shear stress as a polynomial in u as opposed to using a velocity polynomial. The method of Lees and Reeves uses a combination of locally similar and momentum techniques. Both solutions use a coupling equation between the dissipative flow and the isentropic free stream to account for the free interaction. Holt's method of solution, called the "method of integral relations," has the advantage of simplicity.

Experimentally this problem has also attracted the attention of several researchers. One of the earliest and still very important contributions is the work of Chapman, Kuehn and Larson[1] in which several other separated flows are examined. In this work experimental evidence of the free interaction hypothesis is presented, and the influence of Mach and Reynolds numbers on separated laminar transitional and turbulent boundary layers is shown in great detail. Several other investigations examining different aspects of the problem were carried out by Gadd,[7] Bogdonoff and Vas,[8] Needham.[9] Recently Lewis[10] extended Chapman's free interaction correlation to hypersonic adiabatic and cooled walls using Curle's approach. Although a slightly different problem is treated by Sirieix, Mirande and Delery,[11] we will mention their work which is concerned with a detailed investigation of the reattachment region. To illustrate the complexity of this type of flow we will also mention Ginoux's paper[12] which shows the existence of three dimensional effects (generally interpreted as Goertler's vortices) in flows which are essentially two-dimensional.

With the impressive amount of research already undertaken in this field the present experimental investigation finds its justification in the fact that most, if not all, of the preceding work consisted of examining global flow quantities with little attention paid to detailed properties. For example, to our knowledge there has been no final experimental evidence of the existence of a reversed flow, although this is physically unquestionable. We also feel that the computational difficulties encountered by most theoreticians in extending the solution to the reattachment region may not be purely mathematical, but might be due to the fact that the assumptions used are not valid in that region.

Since our purpose was to provide more detailed knowledge of separation phenomena, we sought to measure the thermodynamic and dynamic quantities throughout the flow field using hot wire and pitot probes. Since the recompression region is one of the least understood areas we also attempted to localize the critical points in that region and to interpret their roles in terms of local quantities of the boundary layer in that region, following the work of Siriex, et al.[11]

During the present study the Mach and Reynolds numbers were varied only slightly, the latter always having a value low enough to insure laminar flow over the whole interaction region. The models tested were all adiabatic and allowed for variation of the compression angle $\alpha$ and the downstream conditions. The flow was carefully checked for two-dimensional behavior.

## 2.0 EXPERIMENTAL APPARATUS

### 2.1 Wind Tunnel

The experiments reported here were carried out in the Aeronautical Sciences Division 6" x 6" supersonic wind tunnel at the University of California in Berkeley. This facility (described in extensive detail by Bossel[13]) is a closed type continuous flow tunnel. Stagnation temperature and pressure are adjustable in the range $150 < T_t < 50°F$ and $1.3 < P_t < 35$ psia, which allows a variation of the Reynolds number per foot in the range $1.50 \times 10^5 < Re/ft < 7.35 \times 10^6$ at a Mach number of 2.60. The free stream Mach number in the test section varies by 3% in the streamwise direction over a distance of the same order of magnitude as the length of the model.

This facility is equipped with a schlieren and shadowgraph system which permits ore to observe and photograph the flow.

### 2.2 Models Used

Two models were used for the investigation, both of which were adiabatic.

Model A (see Fig. 2) was essentially used to check for establishment of the flow. It permits continuous variation of the angle $\alpha$ from 7° to 23°. It also allows for changes in the distance from the leading edge to the compression corner from 3 to 4-1/2 inches, and could be used as a flat plate model by removing the ramp mounting. Pressure taps at 1/8 inch intervals were provided on this model.

Model B (see Fig. 3) had the same provision for pressure measurement; however, the ramp position was fixed at 4 inches from the leading edge. The compression angle could be set at the values 9°, 11°, 13°, and 15° by changing the ramp mounting. This model also had an additional

feature--the ramp was constructed of a flexible copper sheet soft-soldered on lateral ribs spaced 1/8 inch apart, which allowed a continuous or a sudden deformation at any angle and at any distance from the compression corner. This deformation could be produced during the run. This feature was used to enable one to change downstream conditions at any point during and after reattachment.

The leading edges of both models were checked carefully and regularly under a microscope; this proved to be beneficial in establishing a laminar boundary layer.

The pressure taps on both models were connected to a Decker differential pressure transducer with a range of ±3 inches of water, which was regularly calibrated against a Dibutyl-phthalate micromanometer. The voltage output of the transducer system was recorded on a Librascope X-Y recorder.

2.3 Probes

Several hot wire and pitot probes were tested and calibrated; however, all the data reproduced in this report were obtained with the probes shown in Fig. 4. These probes were chosen because they indicated a minimum interference with the flow. Both probes had the same mounting --a conical section terminated by a cylinder which fits the arm of the traversing mechanism.

The pitot probe consisted of a piece of stainless steel tubing fitted into the cone at an angle of 30° and bent parallel to the flow 1/2 inch from its tip. The portion of the tube at an angle to the flow is flattened to present minimum disturbance; the mouth of the tube is also flattened for boundary layer measurements (see dimensions in Fig. 4). It was carefully constructed and regularly checked under a microscope.

The hot wire probe had a thin plate fixed to the cone on one end which held one needle parallel to the flow on each side at the other end. This plate was made of two sheets of copper glued together but isolated electrically so that with the needles soft soldered on each face, it served as an electric conductor between the hot wire and the leads to the electronic equipment. This plate could be made very rigid and still very thin (see Fig. 4).

Both probes were mounted on the test section traversing mechanism which permitted positioning on the three axes with an accuracy of ±0.001 inch.

The pitot probe pressure signal was connected to a Decker or a Wianko ±5 psi pressure transducer and the electric signal was recorded on the X-Y recorder where the Y axis was actuated by a voltage input proportional to the distance from the wall of the probe tip.

The hot wire was connected to a heat flux constant temperature anemometer. When the equipment was run in the cold resistance mode the resistance of the unheated wire could be measured with an accuracy of better than ±0.01 Ω. Two other readings from the wire voltage were recorded for very small overheats and since the bridge was at balance the wire currents could be computed with an accuracy of better than $\pm 3 \times 10^{-5}$ amps.

# 3.0 EXPERIMENTAL TECHNIQUES AND DATA REDUCTION

## 3.1 Flow Establishment

The flow to be investigated is the laminar two-dimensional flow over a compression corner. We must then make sure the two conditions are satisfied, namely: two-dimensional and laminar flow. One additional condition is that the boundary layer approaching the corner should be of a Blasius type. In other words, since our model has a leading edge at a finite distance from the corner, we must make sure that the leading edge effect has died out before the interaction occurs.

### 3.1.1 Two-dimensional flow

The width of the test section is 5-1/2 inches, which limits the aspect ratio of the model particularly because the length $\ell$ (see Figs. A and B) cannot be made shorter than a certain length $\ell_{min}$ for the reasons explained in Section 3.1.2. Due to these limitations our aspect ratio $(s/\ell)$ was of the order of 1, which made it important to investigate the two-dimensionality of the flow. An extensive study of this kind has been performed by Lewis,[10] who found that by mounting side plates at equal distances from the center line and by varying this distance, the flow tends to a limit when the aspect ratio becomes of the order of or larger than one. Using different wind tunnel facilities and models, Lewis proved that this limit is actually the desired two-dimensional flow. This result is used in the present investigation. However, since the Mach number used in our case is of order 2.5, an aspect ratio study was carried out. When AR became equal to or larger than one, the limit was attained for a deflection angle $\alpha \leq 15°$. For larger $\alpha$ a considerably larger AR was needed.

As proved by Lewis, we will assume that the limit found does represent the two-dimensional flow.

All of our final data were taken on model B where $\alpha$ was always less than 15°. It was observed (see Fig. 5) that taking out the sideplates altogether does not substantially affect the flow, provided $(s/\ell) \geq 1$. The difference in the pressure distribution observed in that figure near the end of the ramp is due to the appearance of transition when the sideplates were mounted (see subsequent section). It was also observed that transition occurs more easily when the model spans the wind tunnel, presumably because the tunnel wall boundary layer is turbulent and this turbulence is fed to the main flow through the separated bubble in which the velocity is very small.

In the light of these remarks, it was decided to use model B, which does not span the test section and has an aspect ratio of 1.

A final check was performed by applying a thin oil film on the model and observing the oil traces. This showed that there exists a region roughly 3/4 to 1 inch on each side of the centerline where the oil traces were essentially parallel to the main stream. Changing the ramp configuration downstream of the reattachment location did change the oil traces, but the region of two-dimensional flow was still present. It will be assumed in what follows that the ramp length, or more precisely the conditions downstream of reattachment, do not affect the two-dimensional nature of the flow. This is an important point, because the downstream condition effect on the flow is an important part of this study.

3.1.2 Boundary layer ahead of interaction

As stated earlier it is important for our study that the

boundary layer ahead of the interaction be a self-preserving Blasius flow. Model A, which has provision for changing the distance $\ell$ was used first without a ramp and then with the ramp at different locations $\ell$. Pressure distributions in the streamwise direction were taken (see Figs. 6), and it was found that $\ell = 4.00$ inches was sufficient to achieve this condition. This length was used on Model B, and it seems to be the optimum length because $\ell > 4.00$ can have adverse effects on the location of the transition (see next section).

3.1.3 Laminar flow

The last condition to be satisfied is that the flow be laminar before, as well as after, the interaction.

It is a known property of laminar boundary layers that, when observed by a shadowgraph, they exhibit a focusing effect that produces a bright line near their edge. This criterion has been used by Chapman et al.[1] in their investigation. This effect is generally interpreted by the fact that laminar boundary layers have a density profile of small curvature near the edge as compared with a turbulent density profile which exhibits a fuller curvature. This interpretation was checked by hot wire measurements on a flat plate boundary layer. Figure 7 shows two temperature profiles; the curvature of the laminar profile is much smaller than that of the turbulent one. These two profiles exhibited the behavior explained earlier when observed with a shadowgraph, and a confirmation of their laminar and turbulent nature was obtained by a hot wire fluctuation qualitative study. These temperature profiles were obtained from the steady state hot wire measurements explained in a subsequent section.

Several similar tests were carried out; all confirmed the existence of a bright line around the edge of a laminar boundary layer when observed by a shadowgraph. This property was used in all subsequent runs where we could decide on the state of the boundary layer with a quick look at the shadowgraph screen.

In order that transition does not occur in the region of interest in our flow, the tunnel was used at its minimum stagnation pressure; this also had another advantage, because under these conditions the stagnation pressure regulating control was extremely stable and identical free stream conditions could be reproduced in different runs. When transition was desired, a very small increase of stagnation pressure would move the transition upstream to the reattachment region. The stagnation temperature was also set at its minimum value for, even though this had an unfavorable effect on the laminar condition, it assured a very stable free stream temperature during each run. This last point is very important in our case where temperature measurements were also taken.

### 3.2 Flow Measurements

All the information collected in this report was obtained from three basic types of measurements: wall pressure, pitot, and steady state hot wire measurements. The following sections describe all three procedures used in reducing these measurements.

#### 3.2.1 Wall pressure measurements, location of separation and reattachment points

The wall pressure is an important parameter in this type of flow. It was measured as stated earlier with a Decker pressure transducer and the result reconverted in p.s.i. using the transducer's

calibration curve. P was then used mostly in the form $P/P_o$ where $P_o$ was the undisturbed free stream condition. The location of separation and reattachment was found with the help of a technique used by Roshko and Thomke[14] and others.[15,16] It consists of perturbing the flow at each pressure tap and observing whether the perturbation gives an increase or a decrease in the measured pressure. If the perturbation is downstream of the pressure tap, it will create a positive pressure gradient and a higher pressure will be recorded. If a lower pressure is recorded, it means that the perturbation is upstream from the pressure tap. Experimentally this state was realized by bringing a fine wire (diameter of the wire = diameter of the pressure tap hole), attached to the arm of the traversing mechanism, to one side of each pressure tap and noting the pressure each time. The same procedure was then repeated, placing the wire at the other side of the pressure taps, and finally an unperturbed pressure was recorded. The three curves were plotted on the same graph and the point where they intersect is the reattachment point. (At that point, where the flow impinges on the surface, the perturbed pressure and the unperturbed pressure are equal).

This technique was mainly used to pick up the reattachment point, the separation point being located by the thin oil film technique. (Using the fact that the shear after separation is negative and ahead of separation it is positive, the oil will be collected by this action along a line which determines the separation point.)

Finally, the wall pressure measurements were used to investigate the effects of change in conditions at the end of the ramp. This will be explained more extensively in the next chapter.

### 3.2.2 Pitot measurements

The pitot probe described earlier was used to take boundary layer stagnation pressure profiles throughout the interaction region. These measurements were taken for two reasons: (a) to test the hot wire data procedure described in the next section; and (b) to use $P_t$ (instead of wall pressure) along with the hot wire data to investigate the presence of normal pressure gradients in the boundary layer. This latter quantity is difficult to measure directly due to the extremely small size of the region of interaction.

Figure 8 shows a typical Mach number pitot trace ahead of separation; the same figure also shows a Mach number profile computed from hot wire data and wall pressure. Several attempts to correct the pitot data near the wall, using Homann's approach,[17] produced the same results as the hot wire. Hot wire data will replace the pitot results for points near the wall in all that follows. This means that when the stagnation pressure of the pitot is used with the hot wire measurements to check for normal pressure gradients, we will be unable to detect any pressure gradients in the bottom part of the boundary layer (roughly where $M < 0.3$). It is, however, very unlikely that any normal pressure gradient exists there, because as we approach the wall, the streamlines tend to become parallel to it.

### 3.2.3 Hot wire measurements

Due to the size of a hot wire probe, it seemed to us the most practical measuring instrument for separated flows. Thus it was decided that this would be the main source of data for our investigation.

The hot wire measures essentially two quantities: the

resistance of equilibrium (when the wire is not heated) and the heat loss of the wire when it is overheated with respect to the flow around it. These two quantities can be expressed in another form; namely, the temperature of equilibrium $Te_m$ and the Nusselt number $Nu_m$. $Te_m$ is a unique function of $r_{em}$ and the electrical resistivity of the wire, and

$$Nu_m = \frac{q_m\, d}{(Tw_m - Te_m)k_o}$$

where $q_m$ is the heat dissipated in the wire per unit area, $d$ its diameter, $k_o$ the thermal conductivity of the surroundings at the stagnation conditions, and $Tw_m$ the temperature of the heated wire. The subscript $m$ stands for "measured."

These data have to be corrected for end losses, since the wire has a finite length and is soft soldered on each end to the two needle supports. The aspect ratio of our wire was of the order of 300, but, as will be seen later, the correction for end losses can still be appreciable. A derivation of this correction is given by Kovasny[18] and Dewey,[19] and depends essentially on a parameter $S$ given by

$$S = \frac{d}{\ell}\sqrt{\frac{k_w}{k_o}\,\frac{1}{Nu_m}\,\frac{r_w}{r_3}}$$

where $k_w$ is the thermal conductivity of the wire material and $r_w$ and $r_e$ are the resistances of the heated and adiabatic wire. This quantity determines two correction factors $C_N$ and $C_R$ which give us the Nusselt number and recovery ratio for infinite wires:

$$Nu_o = C_N\, Nu_m$$

and

$$\eta = C_R \eta_m$$

where $\eta = T_e/T_t$ ; $\eta_m = Te_m/T_t$ .

$C_N$ is a function of $S$ alone and $C_R$ is a function of $S$ and the recovery temperature of the needle supports. Details on these quantities are given in the Appendix.

Now that our measurements are corrected, we can use the available information on heat loss and recovery temperature of infinite cylinders normal to the stream. Several investigations have shown that for small $M$ and $Re_o$ ($Re_o = \rho ud/\mu_t$) the Nusselt number is a function of these two quantities. Dewey has formulated an empirical equation which represents a curve fit of the existing experimental data. This curve fit is represented by an equation of the form:

$$Nu_o(Re_o,M) = Nu_o(Re_o,\infty) \ \Phi(Re_o,M)$$

where $Nu_o(Re_o,\infty)$ represents the dependence of $Nu_o$ on $Re_o$ when $M >> 1$ and $\Phi(Re_o,M)$ is the departure from this relation when $M$ is no longer very large. These relations are given in the Appendix.

If we call $\eta$ the recovery temperature $T_e/T_t$ we know that in continuous flow $\eta$ is a unique function of $M$; it varies between 1 for $M = 0$ and 0.95 for $M > 2$. In our case, however, using very low free stream stagnation pressures, the fluid can no longer be considered a continuum at the scale of the wire. Dewey has proposed that, if we write

$$\bar{\eta}_* = \frac{\eta - \eta_c}{\eta_f - \eta_c}$$

where $\eta_c$ is the value of $\eta$ at the continuum limit and $\eta_f$ at the

free molecular flow limit, then $\bar{n}_*$ is a unique function of the Knudsen number $Kn_\infty$ for a given M. This was proved by the data of several workers in the field, namely Sherman, Laufer and McClellan, and Dewey. The relations $n_c$ and $n_f$ as a function of M and $\bar{n}_*$ as a function of $Kn_\infty$ are given in the Appendix.

To reduce the hot wire data practically requires an iteration scheme between the end loss correction and the heat loss and recovery factor relations. This computational scheme is shown later in this section. First we will explain the experimental procedures.

Across the two needles of the wire support was mounted a 0.0002" diameter Wollaston wire (Pt,10% Rh). No attempt was made to measure the wire diameter directly and the manufacturer's specifications were adopted. The wire was then annealed to a dull glow for several minutes and brought back to room temperature before it was calibrated. This procedure was carried out for all wires to avoid a great change in the electrical resistivity coefficient after each heating. The wire was then calibrated and the coefficients $\alpha$ and $r_r$ of a relation of the form $T = \alpha r + r_r$ was computed. (In our case the range of temperature is small and $\alpha$ is a constant independent of T). The resistance per foot at 20°C was given by the manufacturer. Using this value, the length of the wire $\ell_w$ was computed ($\ell_w$ was of the order of $5.4 \times 10^{-3}$ ft). The wire was then placed in the test section, and at each point of the boundary layer, two values of overheat coefficients [overheat = $(r_w - r_e)/r_e$] smaller than 0.08 were taken and the voltage drop across the wire was recorded (see previous section). The resistance was then plotted against $i^2$ and the slope computed (actually this was calculated directly without plotting because $i^2$ is a linear function of $r$ for small overheats).

With the calibration curve of the wire and $r_{em}$, $Te_m$ was then computed.

The following computational scheme was programmed and computed on the CDC 6400 of the Computer Center at the University of California at Berkeley.

1. Assume $r_m = 1$ (i.e., $Te_m = T_t$). With this value of $T_e$ compute $k_o$ and $Nu_m$. Compute S and hence $Nu_o$, and from the relation $Nu_o(Re_o,M)$ find M [note that $Nu_o(Re_o,M)$ can also be written $Nu_o(M, T_t, P)$].

2. Once M is known, and using the same value for $T_t$, compute $Kn_\infty$ with either $P_t$ (pitot) or P (wall pressure). Also compute $\eta_f$ and $\eta_c$, and hence find $\eta$.

3. With the value found for M compute $\eta_s$ ($\eta_s = T_s/T_o$ support recovery ratio), and hence find the end loss recovery ratio $C_R$ (see Appendix).

4. Knowing $C_R$ and $r_i$ compute $\eta_m$. Go to 1 and use the computed value for $\eta_m$ instead of $\eta_m = 1$.

This iteration converges very rapidly and usually no changes to the fourth decimal place were observed after the third iteration. In the above computation, a Sutherland's viscosity law was used.

The knowledge of M, $T_t$, and either the wall pressure P or the pitot pressure $P_t$ enabled us to compute all thermodynamic and dynamic quantities in the boundary layer.

## 4.0 RESULTS AND DISCUSSION

The data, collected and reduced by the methods described in the previous sections, will now be analyzed.

We will first give a general description of these results and attempt to relate them to previous experimental and theoretical papers treating this problem. In the second section we will present a detailed analysis of the data and attempt to explain some aspects of this complicated flow in the light of the measurements of local boundary layer quantities which were obtained.

### 4.1 General Discussion. Comparison with Previous Results

The first measurements obtained were the pressure distributions in the streamwise direction for different free stream conditions and compression angles $\alpha$. These measurements show very clearly a pressure rise ahead of the corner, then a constant pressure region that extends to a small distance downstream of the corner, followed by another pressure rise to reattachment and beyond. (See Fig. 5.) This compares qualitatively very well with previous results of Chapman et al., Lewis, etc. Measuring the pressure at separation $p_s$ and the pressure of the plateau region $p_p$ (the separation point being located by the method described earlier), we plotted in Fig. 9

$$\frac{p_p - p_o}{p_o \sqrt{c_f}} \quad \text{and} \quad \frac{p_s - p_o}{p_o \sqrt{c_f}}$$

versus M. This correlation in which $\tilde{c}_f = c_{f_o} / [(c_{f_o})_{R=10^6}]$ has been suggested earlier (see Ref. 1 for more details). On the same figure we also used results from Chapman's investigations (open symbols) which proved the quantitative agreement of our results with his, at least up

to the plateau pressure. The pressure distributions in the second recompression region could not be compared qualitatively with any result because there is no way to correlate the measurements in that region; more details concerning this point will be pointed out in the next section.

The locations of the points of separation and reattachment also proved to be comparable to those found by Chapman. The pressure at the separation point was always slightly more than half of the plateau pressure. The pressure at reattachment cannot be given in terms of the difference between the final pressure and the plateau pressure; in fact, it is wrong to give such a value, for, as shown in 11, and as will also be shown in the next section, the final pressure downstream of the reattachment point can have different values without affecting the main flow.

The hot wire data complemented by either the wall pressure or the pitot total pressure can give us the values of all the thermodynamic and dynamic quantities in the boundary layer. Using the data reduction procedure explained in Section 3.2.3, profiles similar to those in Figs. 10 to 13 were obtained. A total of 20 such profiles were obtained at different streamwise locations for two compression angles and free stream conditions. It is difficult to compare these results with any previous work, for, to our knowledge, no measurements of this kind have been performed. The Mach number profiles across the boundary layer are qualitatively comparable to those obtained by a pitot in (10); however, our measurements seem to be more accurate in the region close to the wall. Figure 10 shows velocity profiles at two stations ahead of separations. Their deformation from a Blasius type profile to a near separation profile is quite clear. Figure 11 shows the static and stagnation enthalpy profiles corresponding to the previous figure. These results

seem to agree qualitatively very well with theoretical predictions. Note that the stagnation enthalpy is not constant across the boundary layer, but goes from a value inferior to the free stream stagnation enthalpy, increases with $y$, overshoots the free stream value and decreases back to this value at the edge of the boundary layer. Note also that the thermal boundary layer is thicker than the velocity boundary layer, although by a small amount. This obviously comes from the fact that the Prandtl number is smaller than one.

Similar remarks can be made on the profiles of Figs. 11 and 12; we can add, however, in the case of Fig. 12 that there is clear evidence there of the existence of a reversed flow. In this figure the minimum value of $u/u'$ corresponds to the zero velocity line; the values of $u/u'$ below this point correspond to the reversed flow, but the hot wire response is independent of the stream direction.

We give these results in this section to draw a general picture of the flow confirming the physical qualitative reasoning proposed in the introduction. A thorough analysis of these data is carried out in the next section.

## 4.2 Detailed Study

### 4.2.1 Existence of normal pressure gradients

Although the assumption of zero normal pressure gradient ($dp/dy = 0$) is always used by theoreticians attempting to solve this problem, no final experimental proof has been advanced which either proves or disproves this basic hypothesis. As we mentioned in earlier sections, our experiments included the indirect computations of $p$ across the boundary layer; the results are shown in Figs. 14a and 14b. Before discussing these results, let us make some pertinent remarks to avoid

misinterpretations due to large errors caused by experimental uncertainties. To compute p the following parameters were measured:

$Re_m$, $Nu_m$ with hot wire probe

$P_t$ with the pitot probe.

However, it was impossible to measure them simultaneously (the traversing mechanism can hold only one probe). So they were measured on two different runs, taking the following precautions:

-- The free stream conditions are identical in the two runs. This was relatively easy to accomplish since the tunnel was mostly used at its lowest stagnation pressures.

-- The position of the probes with respect to the wall was carefully measured using magnifying optics.

The first precaution proved very effective because by taking wall pressure measurements on the two runs they fall within 2.5% from each other. In other words, the flow being measured by the two instruments at different runs was the same. The second precaution was not fully satisfactory; if an error of 0.002" is committed on the distance between the probe tip and the wall this can induce errors on $p_t$ of the order of 30% in the region of large shear. This is due to the fact that in this region all our measured quantities ($Re_m$, $Nu_m$, $P_t$) vary rapidly in the $y$ direction. Note that for this very same reason, the error will be smaller in the regions of low shear, namely near the wall (separated profiles), and around the edge of the boundary layer. Also, we will remember (see Section 3.2.2) that the pitot data near the wall ($M \lesssim 0.3$) was corrected by using the hot wire data along with wall pressure. This means that no pressure gradients are measurable there (using our method).

Figures 14a,b show plots of $p/p_{wall}$ as functions of y at different streamwise locations. A first remark pertaining to what was said above is that $p/p_{wall}$ can be both $\lessgtr$ than 1 inside the boundary layer. This is physically difficult to interpret and may very well be due solely to error contribution.

These plots show a clear tendency toward negative (very small) normal pressure gradients near the edge of the boundary layer mainly at the stations where dp/dx is large (near separation and reattachment, but not in the plateau region). This could be interpreted by the fact that, moving the probes normal to the wall, we will be crossing different compression lines (in the compression waves) that are present in the supersonic upper layer of the boundary layer. However, it can be safely said that no substantial normal pressure gradients are present in the flow we investigated (compression angle $\alpha = 11°$).

Another test based on the previous data was to plot the wall pressure and the pressure at the edge of the boundary layer versus $x/\ell$. Figure 15 shows such a plot and confirms the conclusions drawn above.

On this same figure we also show the pressure distribution as computed from the displacement thickness profile, using Prandtl isentropic compression relationships with the turning angle $\Delta\theta = d\delta_2/dx$. This computed free stream pressure agrees very well with the previous values.

It is worth noting that the wall pressure downstream of reattachment always reaches values larger than the inviscid pressure (downstream of an oblique shock originating at the corner). This is not true for the computed free stream pressures. Although the difference between the two values is very small, it is quite probable that if the compression

angle is made larger, non-negligible normal pressure gradients might exist there. For this reason the only conclusion we can safely propose is that, provided the compression angle is not very large and the boundary layer is laminar, no evidence of the existence of large normal pressure gradients is observed.

4.2.2 Static total enthalpy; wall recovery ratio

Variations of static enthalpy in the $y$ direction are represented in Figs. 16 and 17. Ahead of the interaction $h$ profiles agree very well qualitatively with known data for a flat plate. As the interaction starts, a nearly constant temperature layer starts to develop near the wall. Moving further downstream this layer becomes still thicker, varying roughly like the thickness of the separated bubble. The enthalpy distribution in the region of high shear is still similar to that of an attached boundary layer.

As the flow approaches reattachment, the inverse trend is observed; namely, the region of nearly constant enthalpy becomes thinner while the variation of enthalpy in the high shear region is still qualitatively similar to that of an attached laminar boundary layer. This trend continues after reattachment, but the changes become smaller as we move downstream for the case of a laminar boundary layer. If the boundary layer begins to become turbulent, the enthalpy profile becomes fuller. This, by the way, is also observed in the shadowgraph when the bright region around the edge of the boundary layer begins to disappear. This effect was explained in a previous section.

A closer look at the separated bubble reveals that the enthalpy does not vary in the $y$ direction up to about halfway between the zero velocity line and the separating streamline. Furthermore, the

enthalpy does not vary appreciably in the $x$ direction in a region extending from the beginning to the end of the plateau constant pressure region. (Note that the separated bubble extends both upstream and downstream of the constant pressure plateau region).

The previous remarks suggested a comparison between the adiabatic wall temperature and the equilibrium temperature of a flat plate in a compressible flow at the same local free stream Mach number. Using the value 0.723 for Prandtl number, the theoretical prediction (see Ref. 21) was computed at different stations downstream of the leading edge, using at each station the free stream Mach number measured with the hot wire. Extrapolating the temperature profile to the wall, we find $T_w/T'$ at different stations. Figures 18 and 19 show two plots of $T_w/T'$ compared with the theoretical predictions of Ref. 21.

The agreement is good in general. There is, however, a consistent tendency for a higher measured wall temperature even before the interaction starts. The error may be due largely to the conduction of heat inside the metallic model from regions of high temperatures to cooler regions.

It is safe, however, to assume that the temperature inside the separated bubble is equal to the temperature that the wall would take if the boundary layer remained attached and the local free stream Mach number is that of the separated flow.

4.2.3 Shear stress

The shear stress $\mu(\partial u/\partial y)$ was calculated using Sutherland's viscosity law for $\mu$ and graphically determining $\partial u/\partial y$ from the velocity profiles mentioned earlier. A graphical interpolation was used when computing the shearing stress on the zero velocity line. This procedure is

based on the fact that $u$ is smooth on the zero velocity line and $\partial u/\partial y$ approximated by the tangent has the same value on each side of this point. Due to the inaccuracy in determining $u$ for the low velocities in the separated bubble, the procedure described inevitably induces large errors. The following results should therefore be regarded as more descriptive than quantitative.

Figures 20 and 20 show the variation of

$$\frac{\mu(\partial u/\partial y)}{[\mu(\partial u/\partial y)]_r}$$

with $x$. The reference value $[\mu(\partial u/\partial y)]_r$ is taken to be the shear stress ahead of interaction $(x/\ell = 0.25)$. At this station the boundary layer profile is essentially a Blasius profile.

The variation of this quantity shows the fast decrease in the wall shear stress ahead of separation and after reattachment. In the separated bubble, the changes are much smaller and a clear maximum is observed near the corner.

The increase of the shear after reattachment is different in these two figures. Figure 20 shows a pure laminar reattachment (where the boundary layer stays laminar several boundary layer thicknesses downstream of reattachment), and in Fig. 21 the flow becomes transitional slightly downstream of reattachment. This part of the flow will be discussed in more detail in the last section.

It is clear from the velocity profiles in the separated bubble that the shear stress at the wall is almost equal but opposite to the shear on the zero velocity line. (We used the latter in our graphs because the error in computing it seemed smaller than that which could

result from the uncertainty in the relative positions of the probe with respect to the wall.) Consequently, we can make a qualitative comparison of our results with those of Holt, which seems to confirm the existence of a minimum (negative maximum) of the shear stress near the corner.

4.2.4 Flow inside the separated bubble

At different locations in the streamwise direction, the zero velocity ($u = 0$) point was determined as described in the previous section. This allows us to find at the same $x$ the point A on the mass flux profile which belongs to the separating streamline

$$\int_{0}^{u=0 \text{ point}} \rho u \, dy = \int_{u=0 \text{ point}}^{A} \rho u \, dy$$

This simply says that the mass flux between the $u = 0$ line and the wall is equal to the mass flux between the $u = 0$ line and the separating streamline at the same streamwise position. Figure 22 illustrates the above integration procedure which was carried out graphically by an Amsler integrater. A similar procedure was used to graph streamlines inside the separated bubble.

Figure 23 shows the edge of the boundary layer, the displacement thickness and several streamlines (numbered from 1 to 5) inside the separated bubble.

Defining

$$\overline{\rho u}\,(y = 0, y = y_5) = \frac{1}{y_5} \int_{0}^{y_5} \rho u \, dy$$

and

$$\overline{\rho v}\,(x = x_s, x = \ell) = \frac{1}{\ell - x_s} \int_{x_s}^{\ell} \rho v \, dx$$

The following values give an idea of the magnitude of the quantities of interest inside the separated bubble:

at $x/\ell = 1$

$$\frac{\overline{\rho u}\ (y = 0,\ y = y_5)}{\rho' u'} = 0.028$$

$$\frac{\overline{\rho u}\ (y = y_5,\ \text{separating streamline})}{\rho' u'} = 0.067$$

and along the $u = 0$ line

$$\frac{\overline{\rho v}\ (x = x_s,\ x = \ell)}{\rho' u'} = 0.0018$$

$$\frac{\overline{\rho v}\ (x = \ell,\ x = x_R)}{\rho' u'} = 0.0022$$

As for the velocities, it is clear from Fig. 23 that the largest velocities in the separated bubble are along the separating streamline. In the reversed flow itself, the order of magnitude of $u$ was 3% to 10% of the free stream velocity and that of $v$ (along the $u = 0$ line) above 0.3% to 0.7% of $u'$.

Figure 23 also includes points near the separating streamline that were computed such that the total pressure on these points is equal to the wall pressure at the reattachment point. The fact that these points are quite near the separating streamline means that Chapman's isentropic recompression hypothesis is a valid assumption. A double check concerning this point is also possible. Along the separating streamline we have:

$$\frac{d}{dx}\left(\frac{u^2}{2}\right) = -\frac{dp}{dx} + \frac{\partial \tau}{\partial y}$$

Our result shows that $\partial\tau/\partial y$ is small on the separating streamline (the curvature of the velocity profile is very large there). $\partial\tau/\partial y$ increases when we get near the reattachment but so does $dp/dx$, and it is not

surprising that the isentropic recompression hypothesis is a very good approximation.

It is worth noting here that the accuracy of the hot wire measurements decreases substantially when the velocity becomes small. The above results should then be considered as descriptibe, giving only an order of magnitude of the quantities of interest. Again it must be pointed out that the verification of Chapman's hypothesis is valid provided the angle of compression $\alpha$ is small ($\alpha \leq 13°$), and that the boundary layer is laminar.

4.2.5 Detailed study of the reattachment region

Relatively little is known about the mechanism of reattachment as compared with the separation process where the free interaction theory seems so successful. It seems to us that the main experimental difficulty encountered in that region is the fact that the boundary layer often becomes turbulent when it experiences the negative pressure gradient near recompression. In the following study a special emphasis is put on this point for, as we will see, a transitional reattachment can be radically different from a laminar one.

As stated earlier, Model B, which was used for this study, had a provision for changing the conditions downstream of the reattachment point. More precisely, we could, at a chosen point on the ramp, create a positive or negative pressure gradient of any intensity. Furthermore, this pressure gradient could be imposed either suddenly by a sharp deformation of the wall (deformation spread over a distance of the order of one boundary layer thickness), or gradually (deforming the wall over a distance of several boundary layer thicknesses).

Performing the experiment described above at different

locations downstream of R, we found as in Ref. 11 that there exists a point C, downstream of which the conditions of the flow do not affect the separated flow and the reattachment upstream of $C_1$. The pressure distribution downstream of $C_1$ can lie between two limits $P_{max}$ and $P_{min}$; the range $P_{max} - P_{min}$ increases moving downstream (see Fig. 24).

Disturbing the flow ahead of $C_1$ usually changes by more than 5% the pressure distribution ahead of reattachment. However, a gradual pressure gradient could be applied at some location without disturbing the flow upstream of this location. By a gradual pressure gradient we mean a generally small pressure change spread over a distance larger than three or four boundary layer thicknesses. This can be achieved up to a point slightly downstream of R. We call this point $C_2$, the second critical point. Upstream of $C_2$ any change of the pressure distribution however small or gradual changes the pressure distribution upstream by more than 5%. This result has been observed earlier, and we seem to have the same problem locating the second critical point precisely. This may be largely due to the fact that near the reattachment point the velocities near the wall are extremely small.

It was noted that $C_2$ is usually located at a point on the pressure distribution where $d^2p/dx^2$ starts to become negative; i.e., near the end of the almost linear increase of pressure with x (see Figs. 24 and 25). As in Ref. 11 the point $C_2$ was found to have an interesting property. Writing

$p_{c_2}$ the pressure at $c_2$

$p_p$ the plateau pressure

$x_{c_2}$ the location of $c_2$

$x_{ep}$ the location of the end of the plateau constant pressure region

and plotting $(p_{c_2}-p)/(p_{c_2}-p_p)$ versus $(x_{c_2}-x)/(x_{c_2}-x_{ep})$ (Fig. 26), we see that we can correlate the pressure distributions found at different free stream conditions up to $C_2$. This figure also includes data from previous investigations where we estimated the location of $C_2$ using the property mentioned previously.

Noting that the pressure distribution slightly downstream of the plateau pressure increases linearly up to $C_2$, we ask ourselves if and how this slope could be related to the free stream conditions and model geometry. In order to compare data from different sources instead of looking at $p$ versus $x/\ell$ distribution, it is more meaningful to look at $p$ versus $Re_x$. The most obvious parameter on which the slope of $p$ might depend is the angle at which the separated free shear layer impinges on the ramp. Call this angle $(\alpha-\beta)$, where $\beta$ is the angle of the free shear layer with respect to the flat plate.

Figure 32 shows the dependence of the slope of $p$ versus $Re_x$ on $(\alpha-\beta)$ (some of the points were taken from other references for larger $\alpha$ and M). This figure suggests a rather simple dependence; however, it should not be regarded as an accurate correlation for the pressure distribution near the reattachment point. It should be noted here that $\beta$ is a function of the plateau pressure, which is itself a function of $M, Re_{x_o}$, so that the quantity $(\alpha-\beta)$ includes both the free stream conditions and model geometry. The points of Fig. 32 that are computed from Ref. 1 correspond to leading edge separation; the fact that they fit well with the other points suggests that the mechanism of reattachment does not depend strongly on the mechanism that induced separation, but rather on the mixing process after separation.

Although the location of $C_2$ could not be given with an accuracy of better than plus or minus one boundary layer thickness, it was consistently found that its distance from the reattachment point did not change very much with small changes in the free stream Reynolds number. Such was not the case for $C_1$; it was observed that a small change of $Re_o$ could move $C_1$ several boundary layer thicknesses even when the pressure distribution in the separated flow did not change by more than 3%. This casts some doubts about the critical importance of such a point on the reattachment process. Furthermore, it was noticed that $C_1$ moves downstream with increasing $Re_o$. This suggested a relation of this point with the occurrence of transition.

Figure 27 shows velocity profiles downstream of the reattachment point. Note that the boundary layer does not change appreciably over a distance of about ten boundary layer thicknesses. In the flow that corresponds to these profiles, the critical point $C_1$ was not detectable before the end of the ramp.

Figure 28 shows transitional velocity profiles downstream of the reattachment point. The flow upstream of the second critical point was identical to that corresponding to Fig. 26. However, in this new case the first critical point was located and had the properties described earlier. The last two figures suggest that the physical meaning of this point is that the boundary layer has picked up enough momentum to enable it to overcome finite sudden pressure gradients. Figures 29 and 30 further support this argument. Looking at the relative slopes of the displacement thickness with boundary layer edge, we see that in a transitional flow there is substantially more momentum entering the boundary layer. The location of the first critical point could thus be related

to the occurrence of turbulence.

Attempts to relate the location of the first critical point in terms of some parameter involving mean quantities of the boundary layer yielded Fig. 31. In this figure we chose the mean Mach number defined as:

$$\bar{M} = \frac{1}{\delta} \int_0^{\delta} M \, dy$$

as this parameter, and we plotted $\bar{M}$ versus $x/\ell$ for laminar and transitional reattachment. Even though $\bar{M}$ becomes larger than one in the transitional case, it is clearly not the parameter to distinguish between the subcritical and supercritical conditions of the Crocco Lees, Lees and Reeves theory. The theoretical parameters of these theories would indicate a subcritical condition for an adiabatic Blasius profile. This is not the case of $\bar{M}$ ahead of separation in Fig. 31.

The fact that the first critical point was not detectable before the end of the ramp in the case of pure laminar reattachment, does not necessarily imply the non-existence of this point. However, if this point exists it will be at several score boundary layer thicknesses from the reattachment. Furthermore, there is some doubt as to the possibility of a laminar reattaching boundary layer becoming "supercritical" (in the sense of the theories mentioned above) because when the boundary layer is fully rehabilitated, it will tend to become a Blasius profile, and this profile is known to be subcritical. This remark is clearly not valid for a laminar wake flow where the mean properties of the boundary layer after the rear stagnation point will eventually imply a supersonic behavior. This will also be the case for a turbulent flow where the distance over which the boundary layer receives enough momentum to rehabilitate itself will be substantially smaller and $C_1$ close to $C_2$.

Figures 29 and 30 also show a clear neck in the boundary layer thickness when the flow is transitional; this is not observed for pure laminar reattachment where the boundary layer decreases very slowly after the second critical point and reaches an almost constant thickness for boundary layer thicknesses downstream.

To state briefly the results of this section, we can say:

1. There exists a critical point $C_2$ slightly downstream of reattachment which plays an important role in the mechanism of reattachment (see Fig. 26) and which marks the beginning of the rehabilitation of the reattached boundary layer.

2. If transition to turbulent flow occurs downstream of $C_2$, another critical point $C_1$ can be located. This point has the property that downstream of it the conditions do not affect the flow upstream, provided they lie in some range. $C_1$ cannot be located for laminar flow (at least close to R), and there is doubt about its theoretical importance for reattaching laminar boundary layers.

## 5.0 CONCLUSIONS AND SUGGESTIONS FOR FUTURE WORK

A detailed experimental study has been made of the two--imensional laminar flow over a compression corner with Mach numbers around 2.5. The following conclusions were reached.

1. For a small compression angle $\alpha$ ($\alpha \leq 13°$) and a laminar boundary layer there is no evidence of appreciable normal pressure gradients in the boundary layer ahead, during, and after interaction.

2. The separated bubble has sensibly constant enthalpy equivalent to the wall enthalpy of a flat plate with attached boundary layer and an equivalent free stream Mach number.

3. The shear stress along the $u = 0$ line is usually not larger than 10% of the shear stress at the wall ahead of the interaction. The maximum of the shear stress along the $u = 0$ line occurs near, but slightly downstream of the corner.

4. Evidence of a reversed flow about 10% the velocity of the free stream exists. The maximum of $u$ in the separated bubble is along the separating streamline, and is always smaller than half the local speed of sound. Provided $\alpha$ is small and the boundary layer is laminar, the assumption of isentropic recompression is a good approximation.

5. Two critical points were located in the separated region. One of them seems to be greatly affected by the occurrence of transition and is not detectable for pure laminar flow over a distance of more than 15 boundary layer thicknesses downstream of reattachment. The other is consistently near the reattachment point and seems to play an important role in the reattachment recompression process.

Due to the limitations mentioned earlier, some aspects of the problem could not be investigated. Future work based on the same techniques could

clarify the following points:

1. Existence of normal pressure gradients and validity of isentropic recompression along dividing streamline when $\alpha$ is no longer small and/or when the boundary layer is turbulent.

2. Attempts to locate the first critical point with a longer ramp. Test the critical importance of this point, if any.

3. Detailed enthalpy study for the case of highly cooled wall.

## REFERENCES


1. Chapman, D. R., D. M. Kuehn and K. L. Larson, "Investigation of Separated Flows in Supersonic and Subsonic Streams with Emphasis on the Effect of Transition," NACA Rept. 1356 (1958).
2. Curle, N., "The Effects of Heat Transfer on Laminar Boundary Layer Separation in Supersonic Flow," Aero. Quarterly XII, 309-335 (1961).
3. Gadd, G. E., "A Theoretical Investigation of Laminar Separation in Supersonic Flow," J. Aeronaut. Sci. 24, 759-771 (1957).
4. Hakkinen, R. J., I. Greber, L. Trilling, and S. S. Abarnabel, "The Interaction of an Oblique Shock Wave with a Laminar Boundary Layer," NASA Memo 2-18-59W (1959).
5. Holt, M., "Separation of Laminar Boundary Layer Flow Past a Concave Corner," in AGARD Separated Flows, Part 1 (1966), pp. 70-87.
6. Lees, L. and B. L. Reeves, "Supersonic Separated and Reattaching Laminar Flows. 1. General Theory and Application to Adiabatic Boundary Layer/Shock Wave Interactions," AIAA J. 2, 1907-1920 (1964).
7. Gadd, G. E., "An Experimental Investigation of Heat Transfer Effects on Boundary Layer Separation in Supersonic Flow," J. Fluid Mech. 2, 105-122 (1957).
8. Bogdonoff, S. M. and I. E. Vas, "Some Experiments on Hypersonic Separated Flows," ARS J. 32, 1564-1572 (1962).
9. Needham, D. A., "Laminar Separation in Hypersonic Flow," Ph.D. Thesis, University of London (1965).

10. Lewis, J. E., "Experimental Investigation of Supersonic Two Dimensional Boundary Layer Separation in a Compression Corner with and without Cooling," Ph.D. Thesis, Calif. Inst. of Tech. (1967).

11. Siriex, M., J. Mirande and J. Delery, "Experiences fondamentales sur le recollement turbulent d'un jet supersonique," in AGARD Separated Flows, Part 1 (1966), pp. 353-342.

12. Giroux, J. J., "The Existence of Three Dimensional Perturbations in the Reattachment of a Two Dimensional Supersonic Boundary Layer after Separation," AGARD Report 272 (1960).

13. Bossel, H., "Flow Studies and Turbulence Measurements in the Hesse 6-inch Supersonic Wind Tunnel," Univ. of Calif. Aero. Sciences Rept. AS-67-2 (1967).

14. Roshko, A., and G. J. Thomke, "Observation of Turbulent Reattachment Behind an Axisymmetric Downstream Facing Step in Supersonic Flow," AIAA J. 4, 975-980 (1966).

15. Sfeir, A. A., "Supersonic Flow Separation over a Backward Facing Step," Univ. of Calif. Aero. Sciences Rept. AS-66-18 (1966).

16. Kuehn, D. M. and D. J. Monson, "Boundary Layer Separation and Reattachment with and without Ablation," in AGARD Separated Flows, Part 1, (1966), pp. 121-145.

17. Homann, F., "The Effect of High Viscosity on the Flow Around a Cylinder and Around a Sphere," Univ. of Calif. Tech. Rept. HE-150-88 (1951). (Translation from the German b D. C. Ipsen.)

18. Kovasznay, L.S.G.,"Hot Wire Method," in Physical Measurements in Gas Dynamics and Combustion, High Speed Aerodynamics and Jet Propulsion, Princeton Series, Vol. 9, Princeton Univ. Press, Princeton, N. J. (1954), pp. 219-241.

19. Dewey, C. F., Jr., "Hot Wire Measurements in Low Reynolds Number Hypersonic Flows," ARS J. 12, 1709-1717 (1961); also, "A Correlation of Convective Heat Transfer and Recovery Temperature Data for Cylinders in Compressible Flow," J. Heat & Mass Transfer 8, 245-252 (1965).

20. Yanta, W. J., "A Hot Wire Stagnation Temperature Probe," Naval Ordnance Lab. Rept. NOL TR 68-60 (1968).

21. Schlichting, H., Boundary Layer Theory, Sixth Edition, McGraw Hill Book Co., New York (1968), pp. 317-318.

22. Nielsen, J. N., Lynes, L. L., and Goodwin, F. K., "Theory of Laminar Separated Flow on Flared Surfaces Including Supersonic Flow with Heating and Cooling, in AGARD Separated Flows, Part 1, (1966), pp. 31-68.

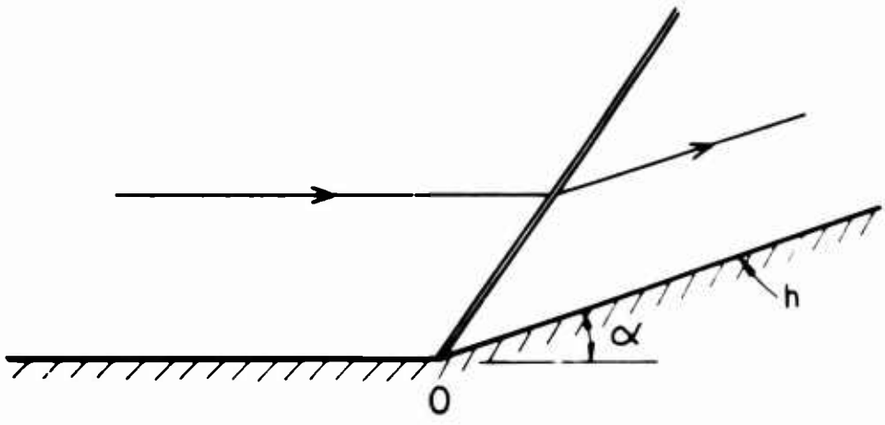


a INVISCID

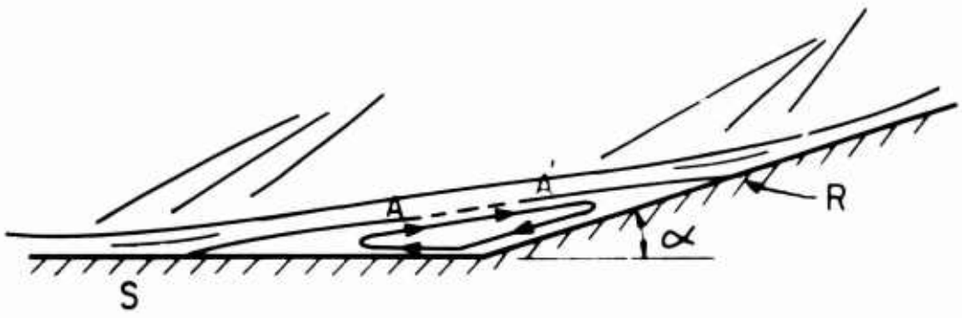


b VISCOUS

FIG. 1 FLOW OVER A COMPRESSION CORNER

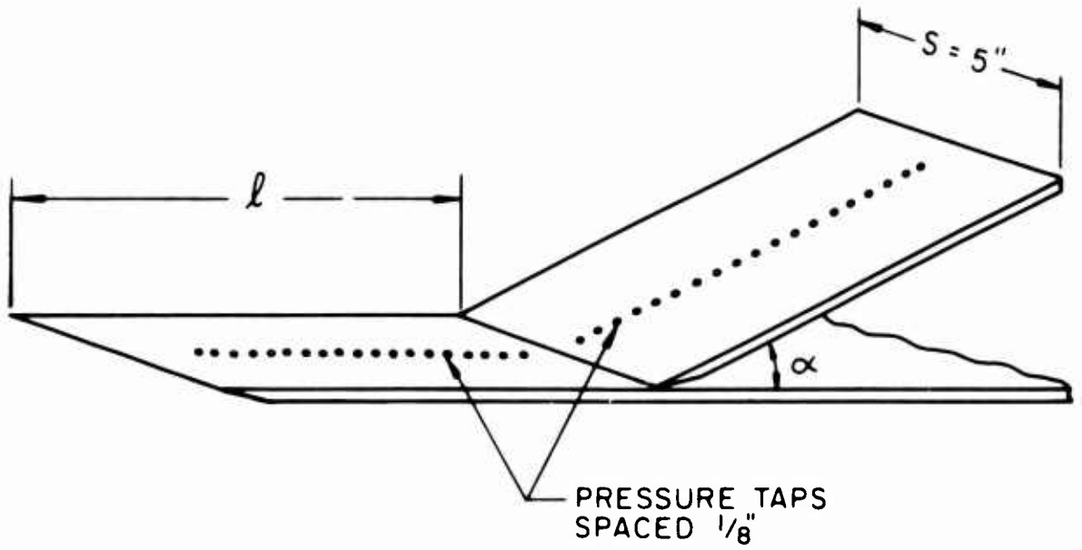


α VARIES FROM 7° TO 23°
ℓ VARIES FROM 3" TO 5"

FIG. 2 MODEL A

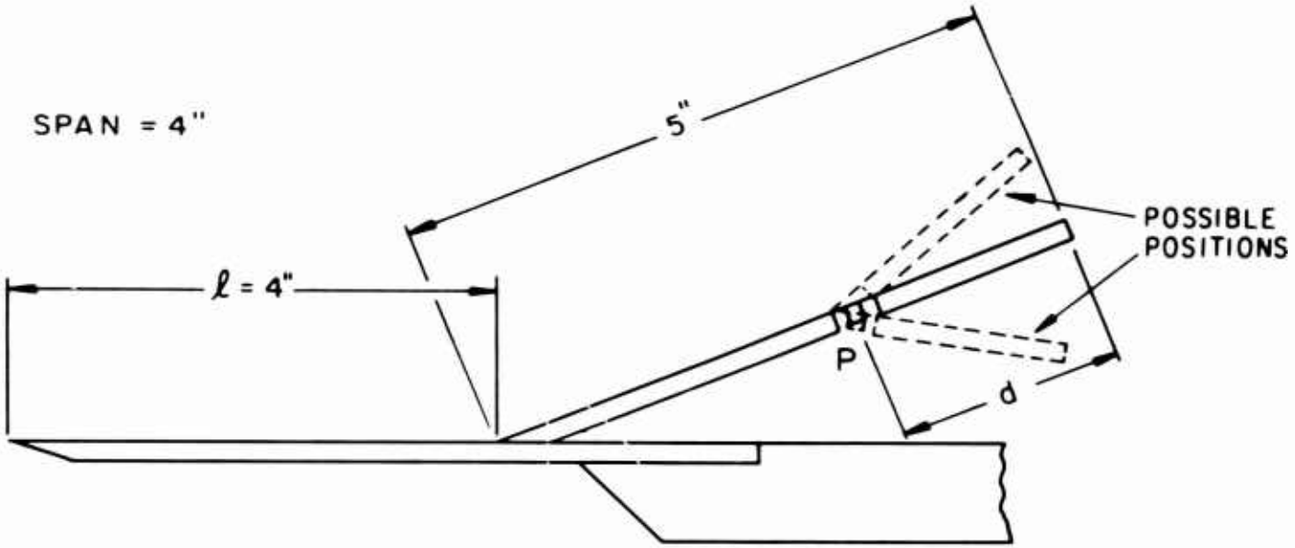


d CAN VARY FROM $\frac{1}{8}$" TO 3"

PRESSURE TAPS ALONG CENTERLINE EVERY $\frac{1}{8}$"

FIG. 3 MODEL B

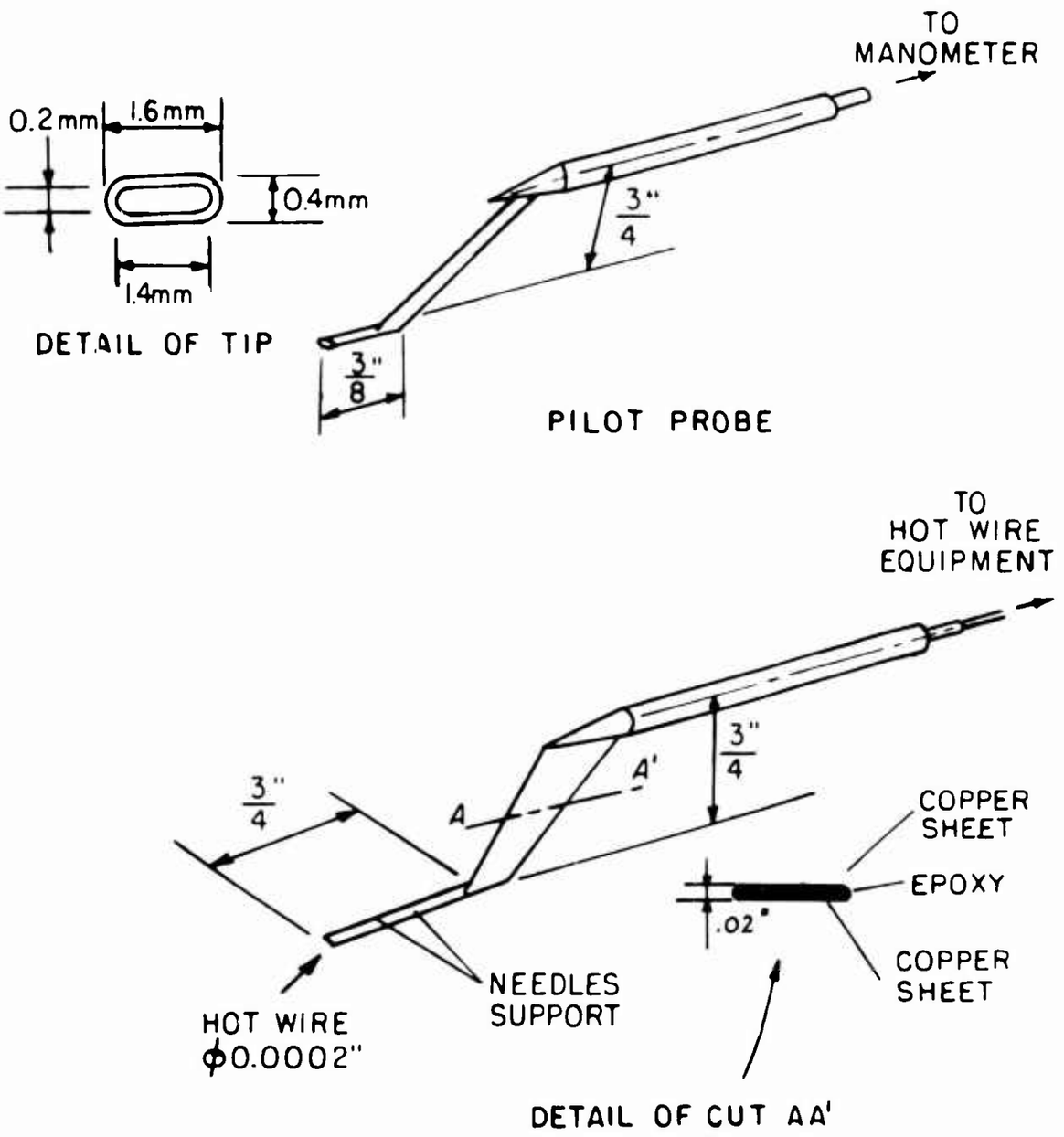
TO
MANOMETER
0.2 mm
1.6mm
0.4mm
1.4mm
DETAIL OF TIP
3"
4
3"
8
PILOT PROBE
TO
HOT WIRE
EQUIPMENT
3"
4
A'
3"
4
A
COPPER
SHEET
EPOXY
.02"
COPPER
SHEET
NEEDLES
SUPPORT
HOT WIRE
ϕ0.0002"
DETAIL OF CUT AA'

FIG. 4 PROBES

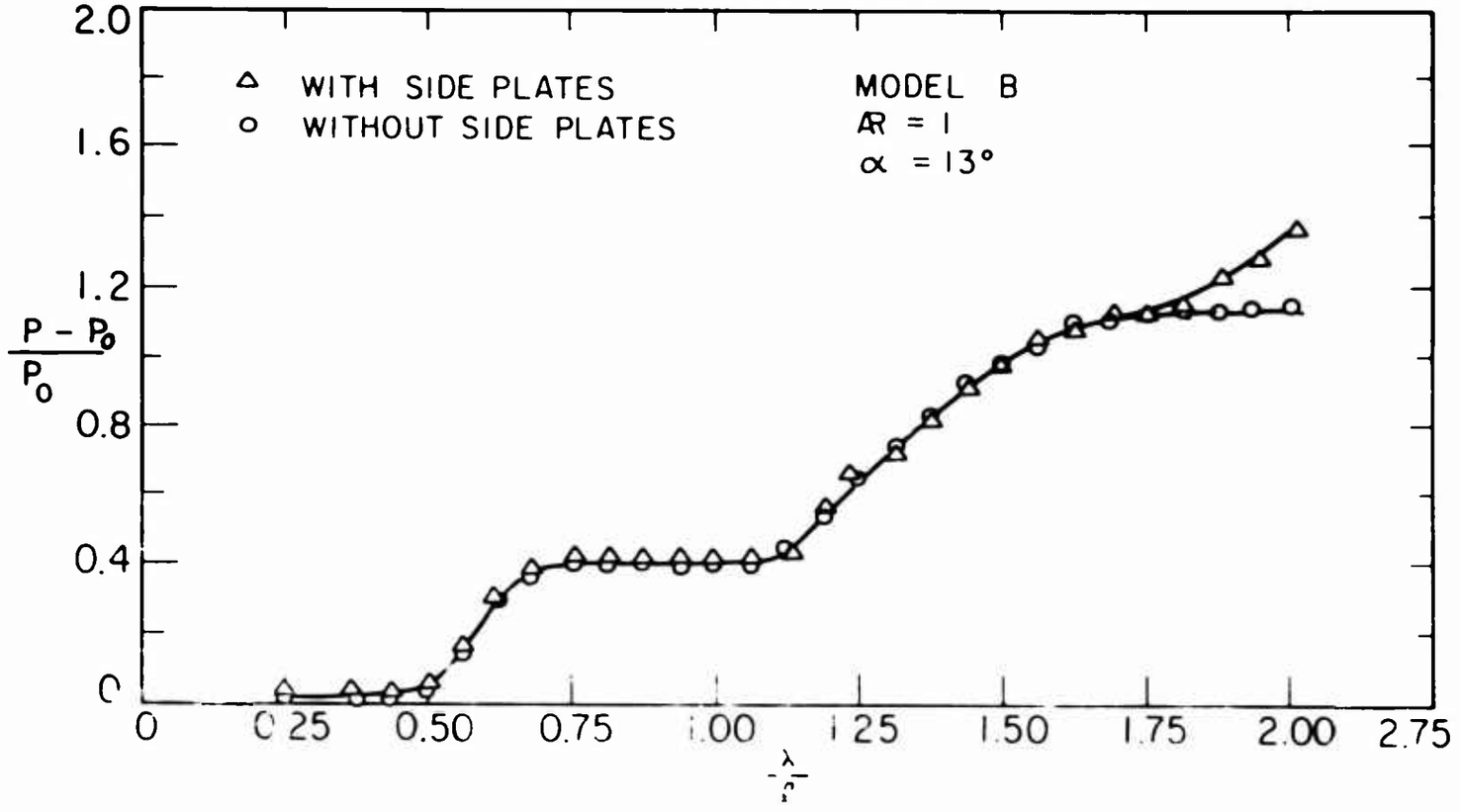


F[illegible] INFLUENCE OF [illegible] PLATES WHEN AR = 1

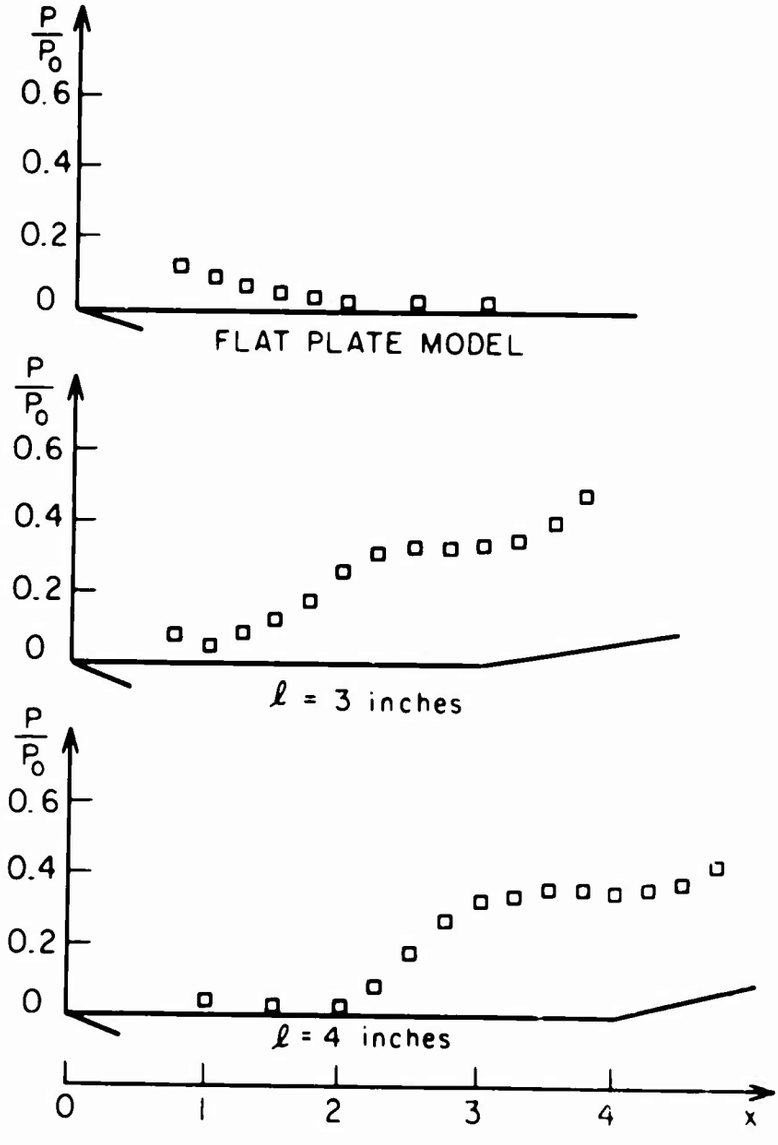


FIG. 6 LEADING EDGE EFFECT

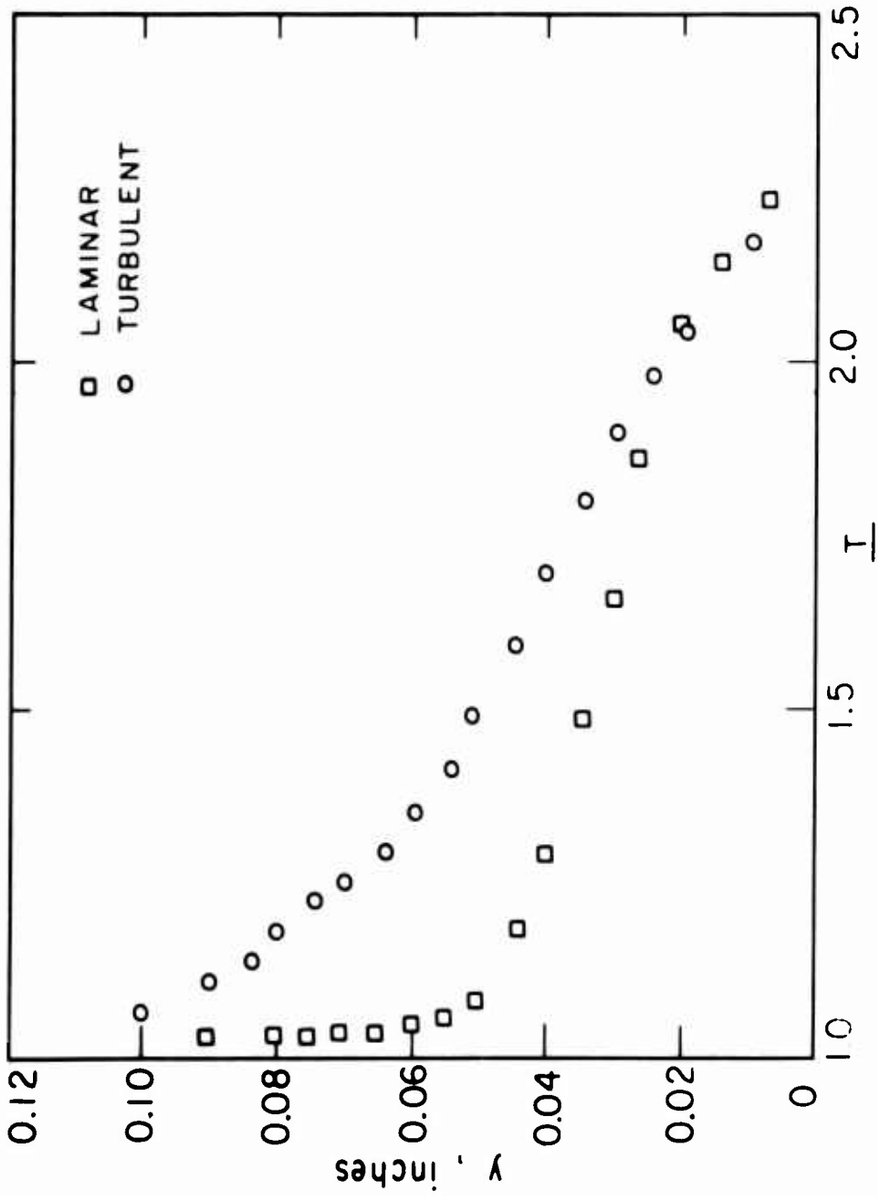


FIG. 7 LAMINAR AND TURBULENT TEMPERATURES PROFILES PRESEPARATION

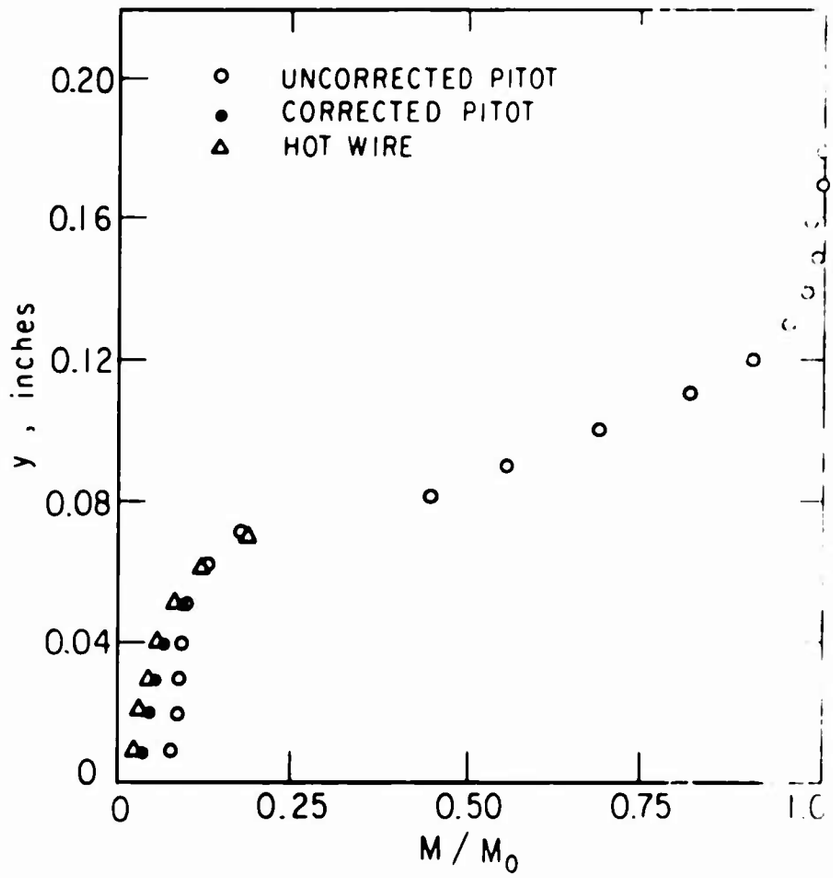


FIG. 8 UNCORRECTED AND CORRECTED PITOT DATA

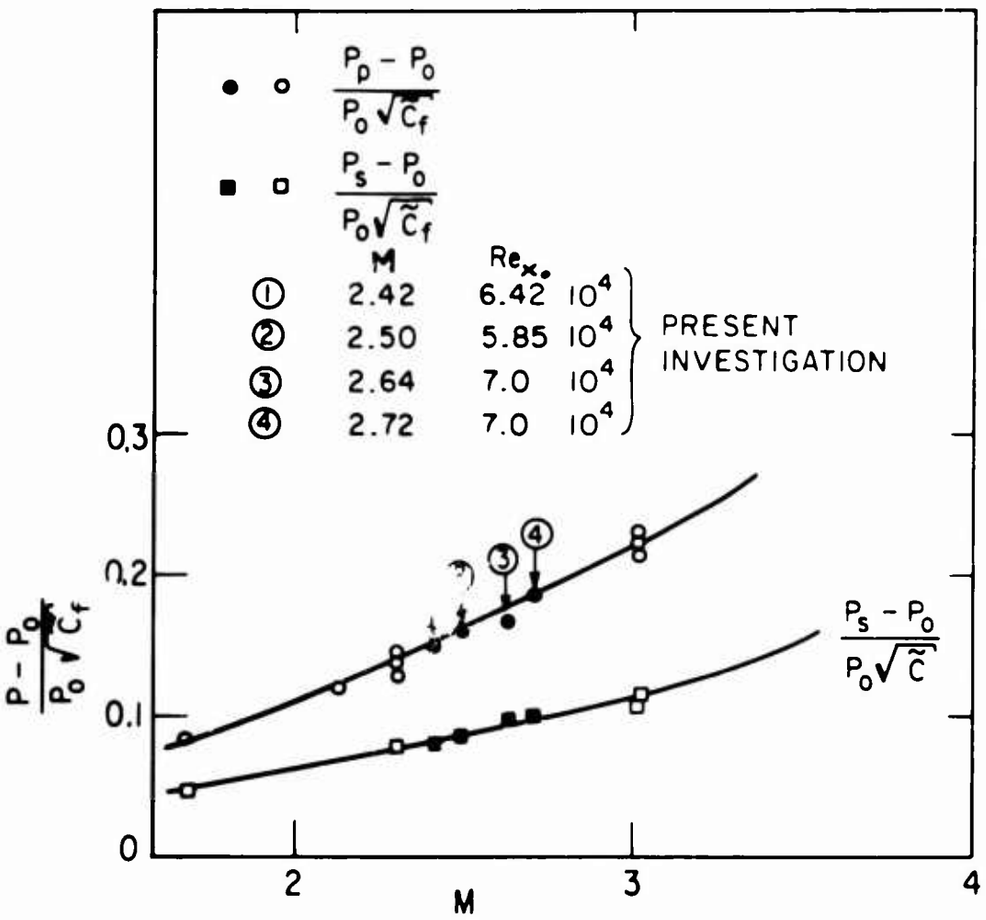


FIG. 9 CHAPMAN'S CORRELATION FOR SEPARATION AND PLATEAU PRESSURES

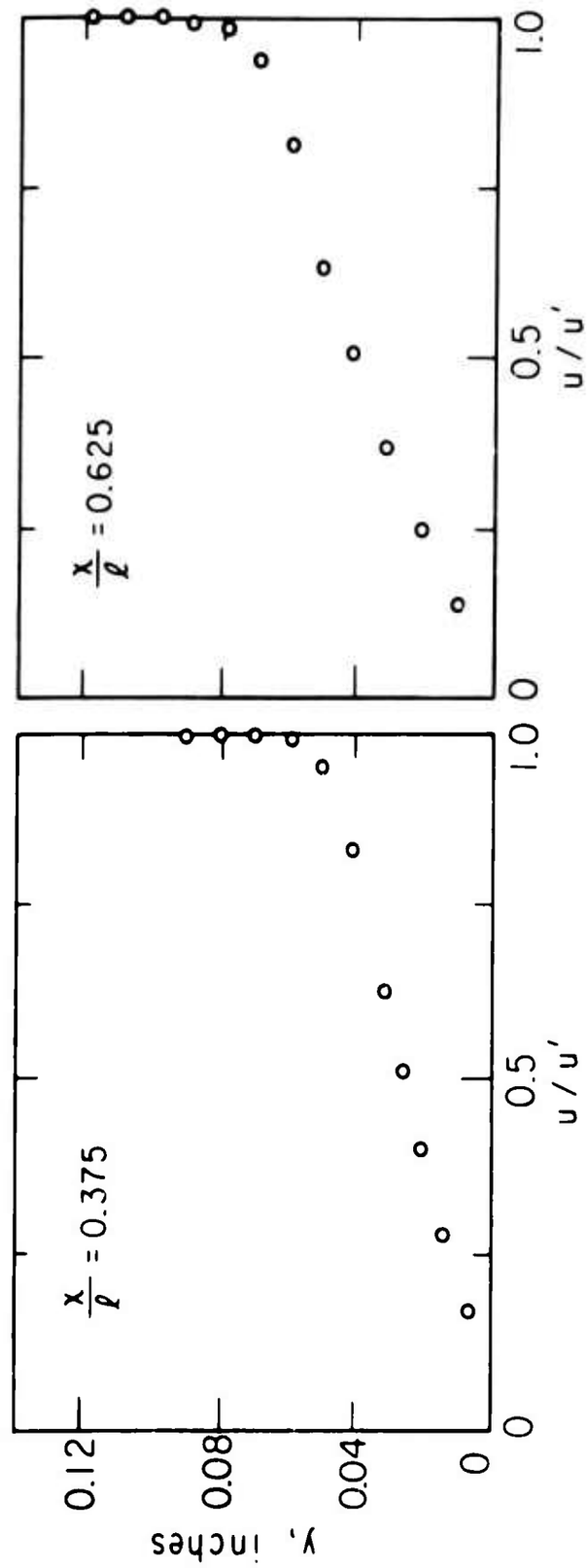


FIG. 10 VELOCITY PROFILES OF TWO STATIONS AHEAD OF SEPARATION

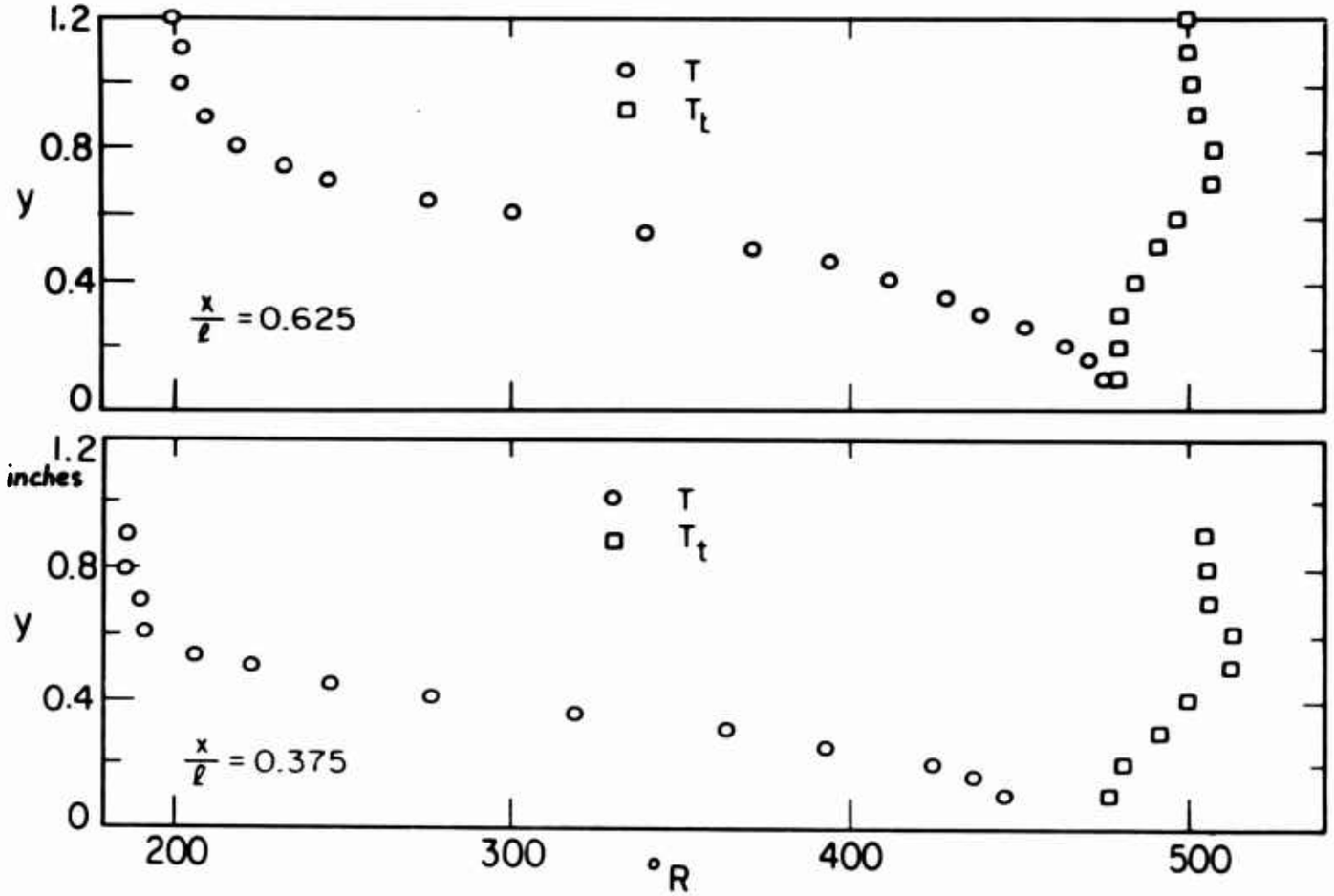


FIG 11 TEMPERATURE PROFILES AT TWO STATIONS AHEAD OF SEPARATION

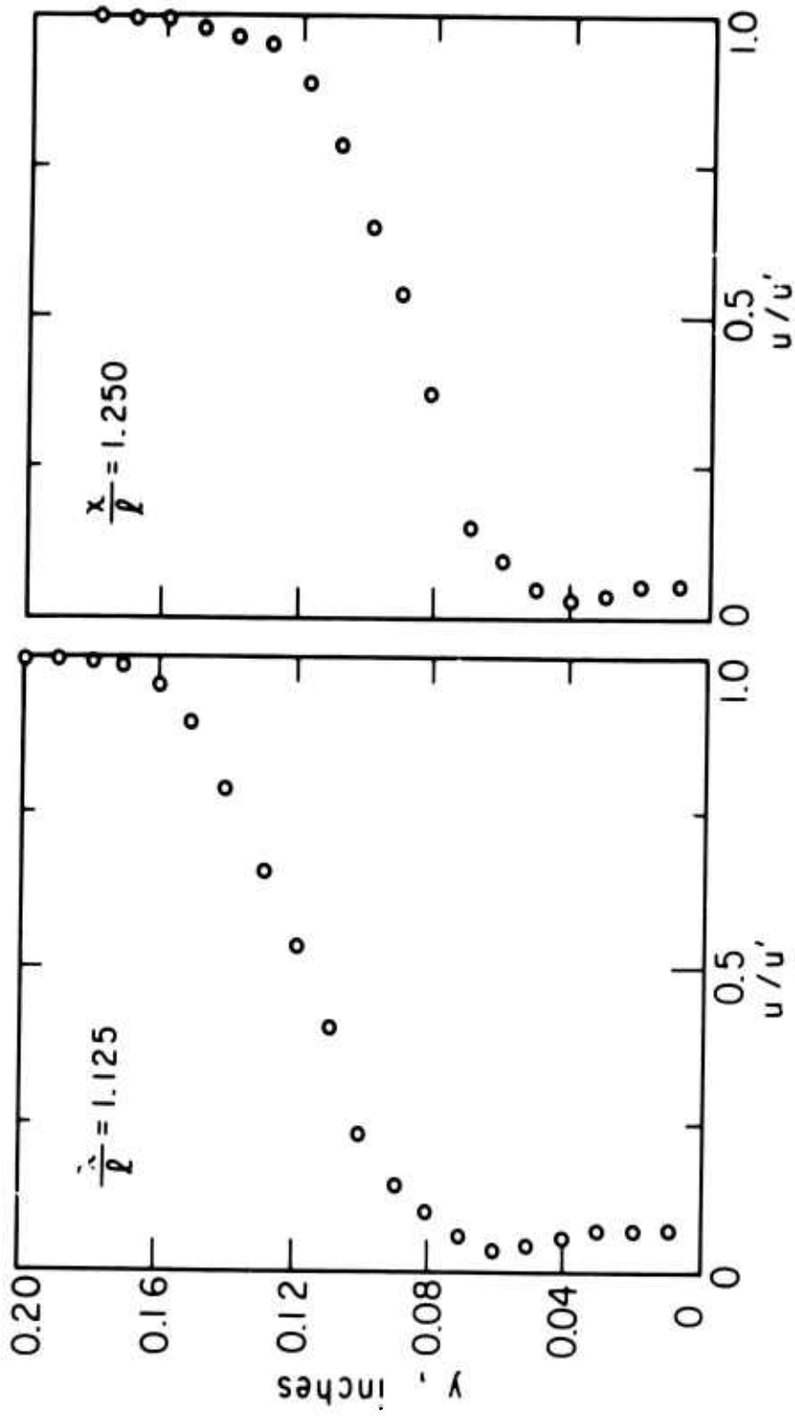


FIG. 12 VELOCITY PROFILES IN THE SEPARATED REGION

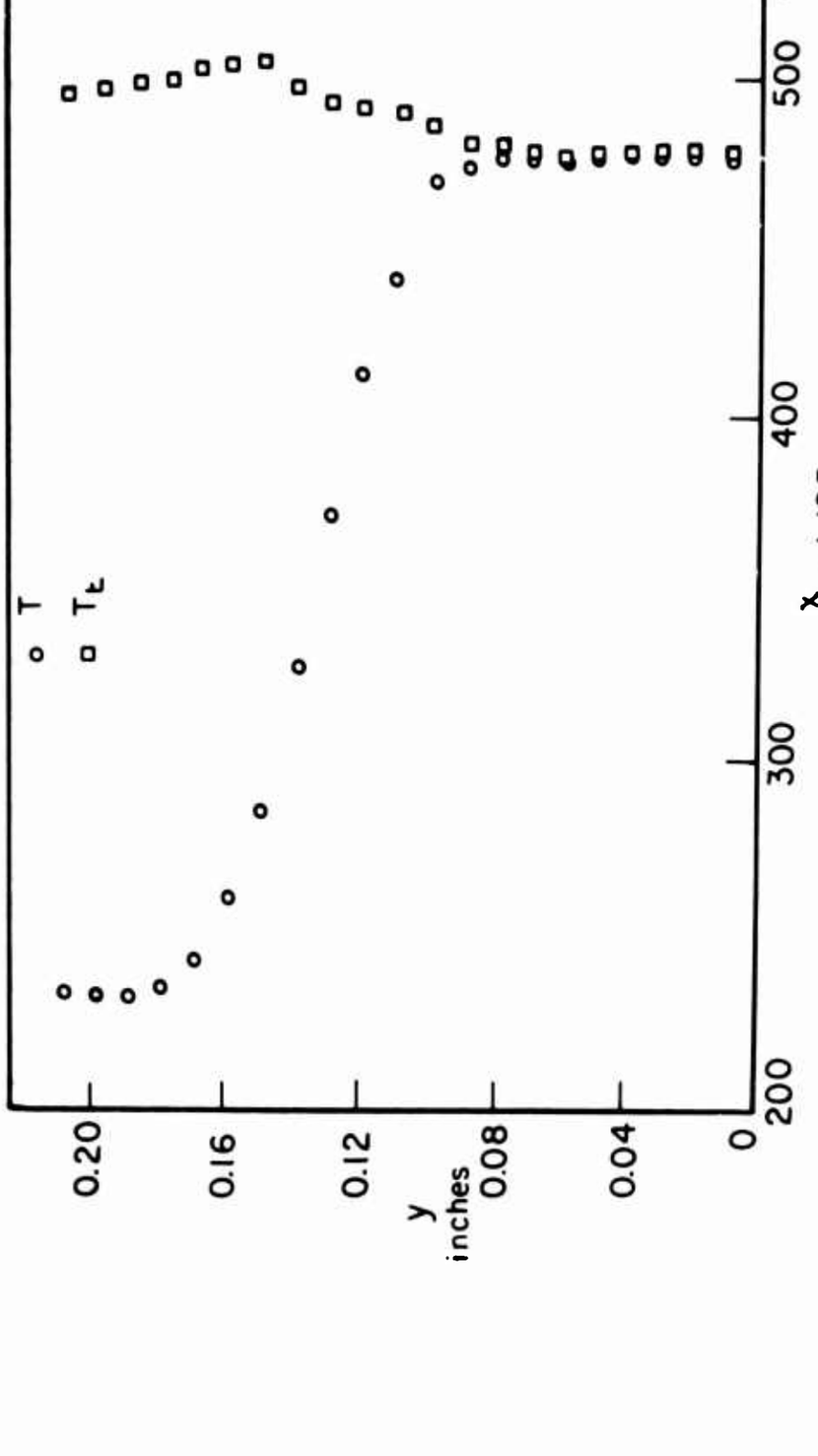


FIG. 13 TEMPERATURE PROFILES IN THE SEPARATED REGION

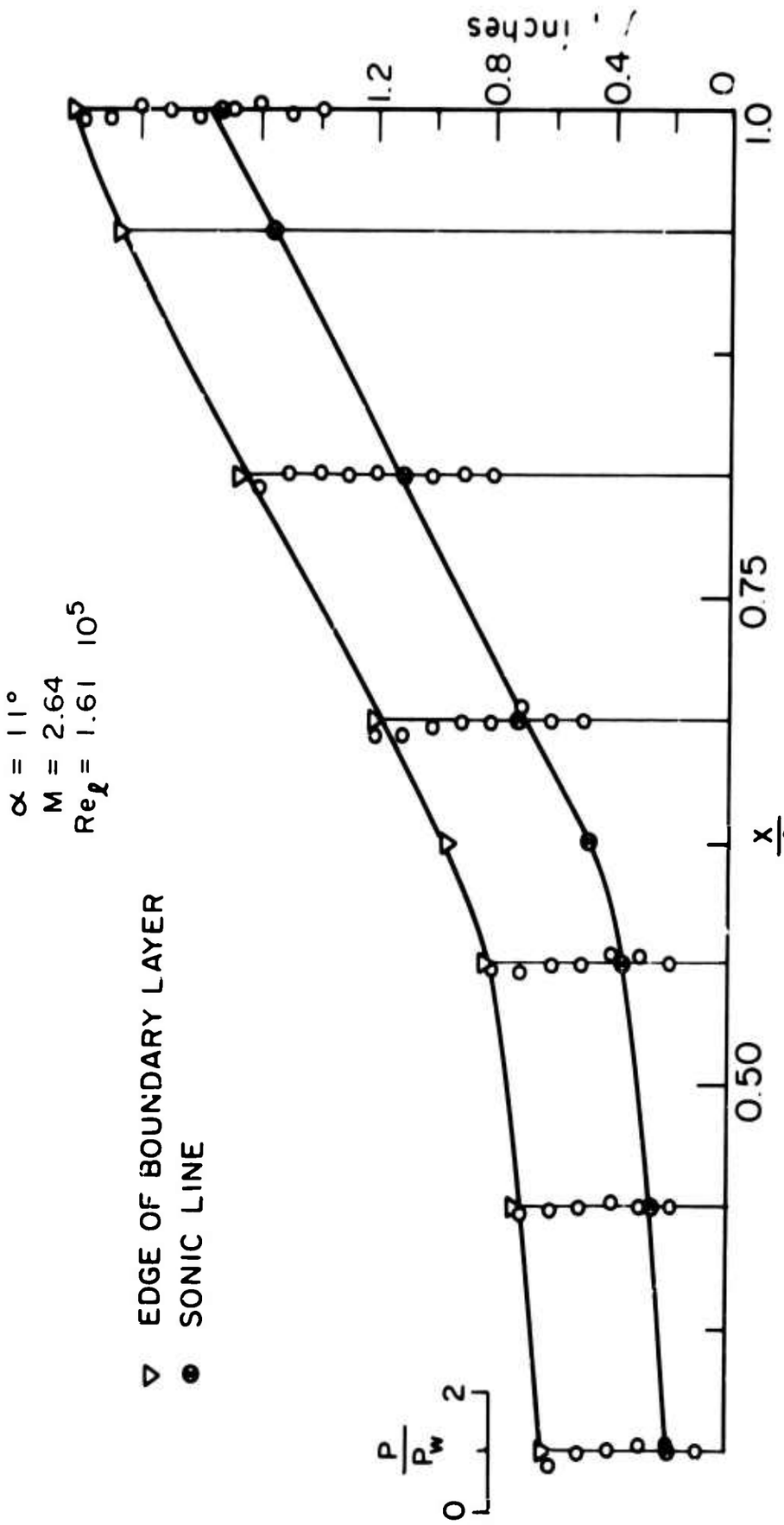


FIG 14a STATIC PRESSURE IN BOUNDARY LAYER

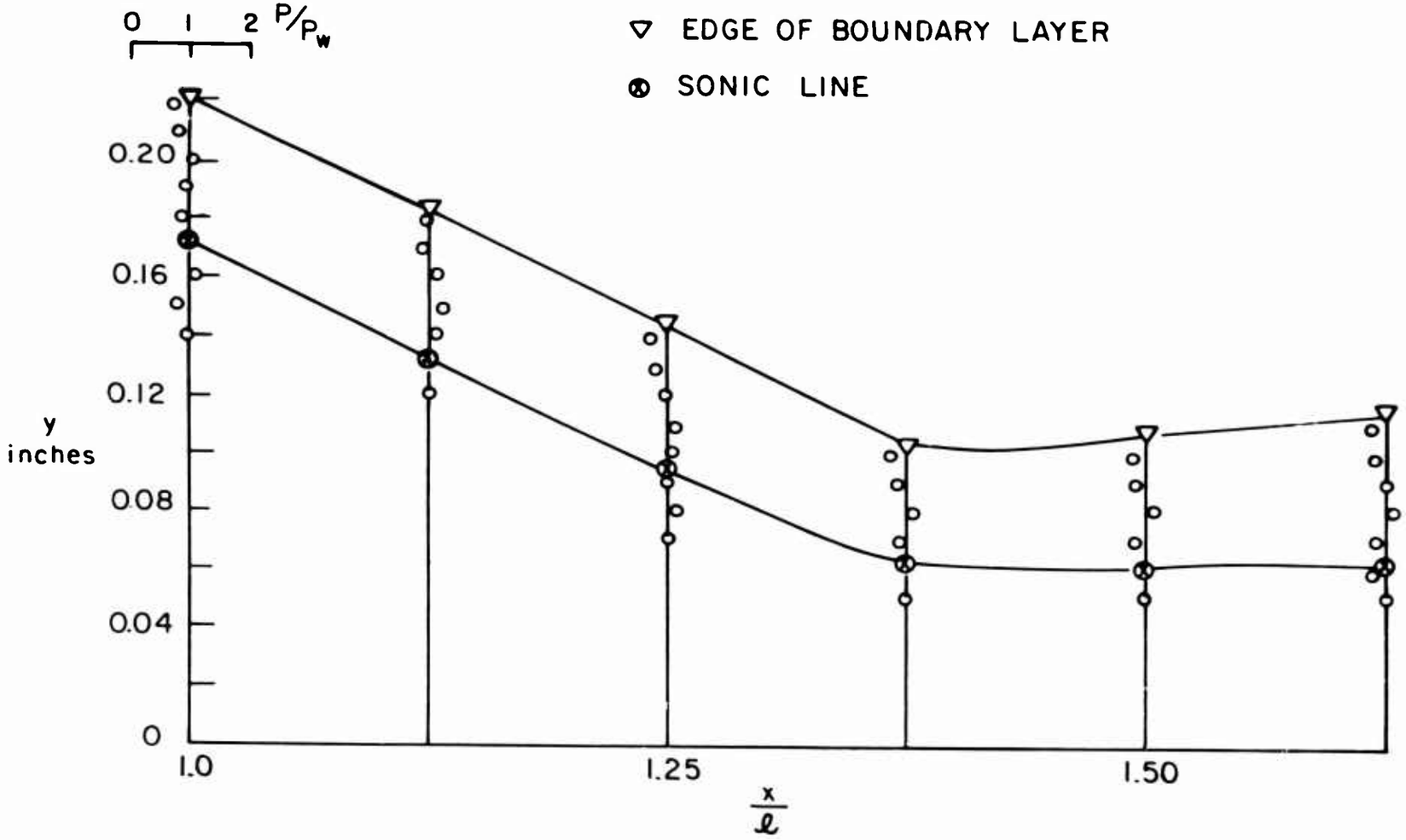


FIG. 14b STATIC PRESSURE IN BOUNDARY LAYER ( CONTINUED )

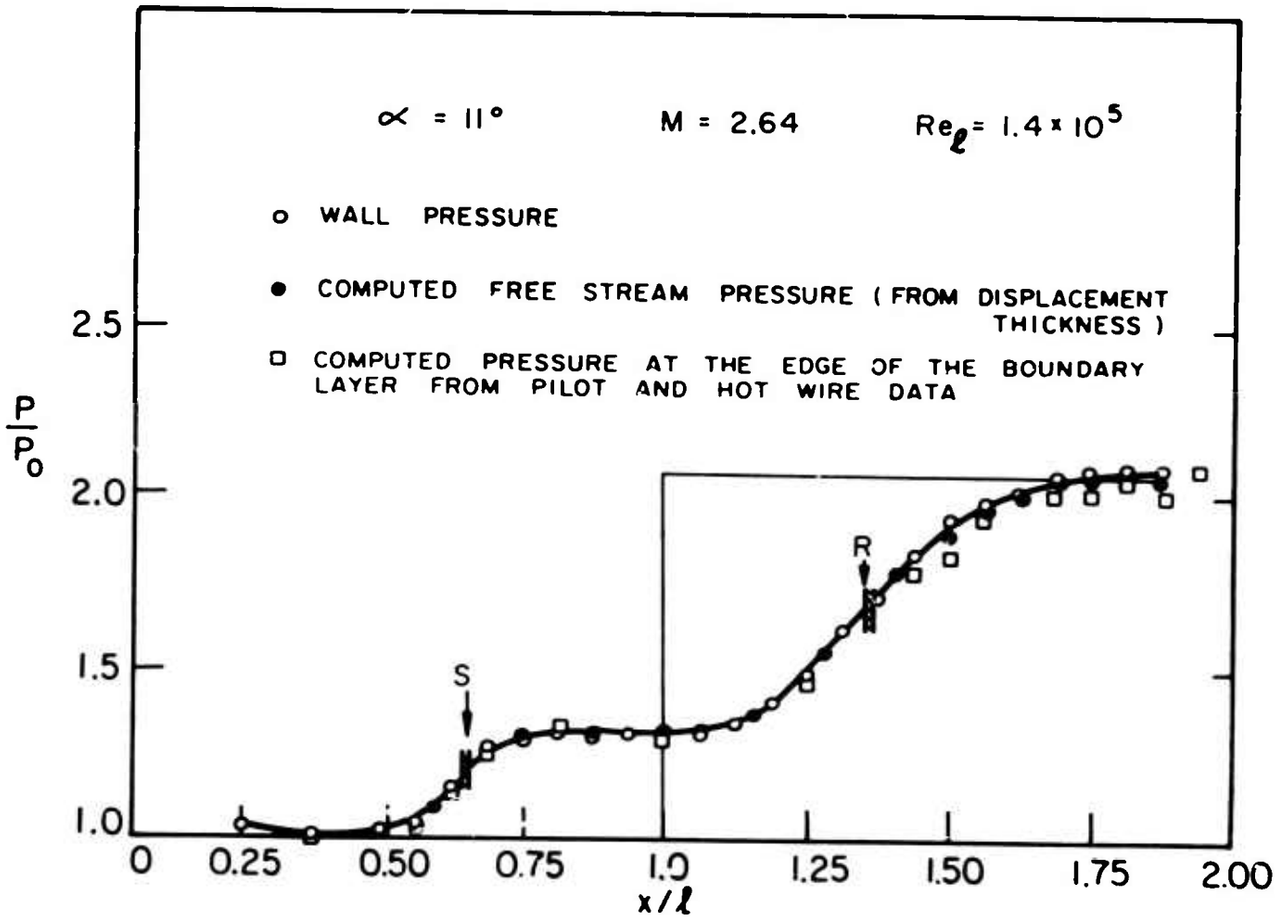


FIG. 15 COMPARISON OF WALL PRESSURE WITH COMPUTED PRESSURE OF THE EDGE OF THE BOUNDARY LAYER

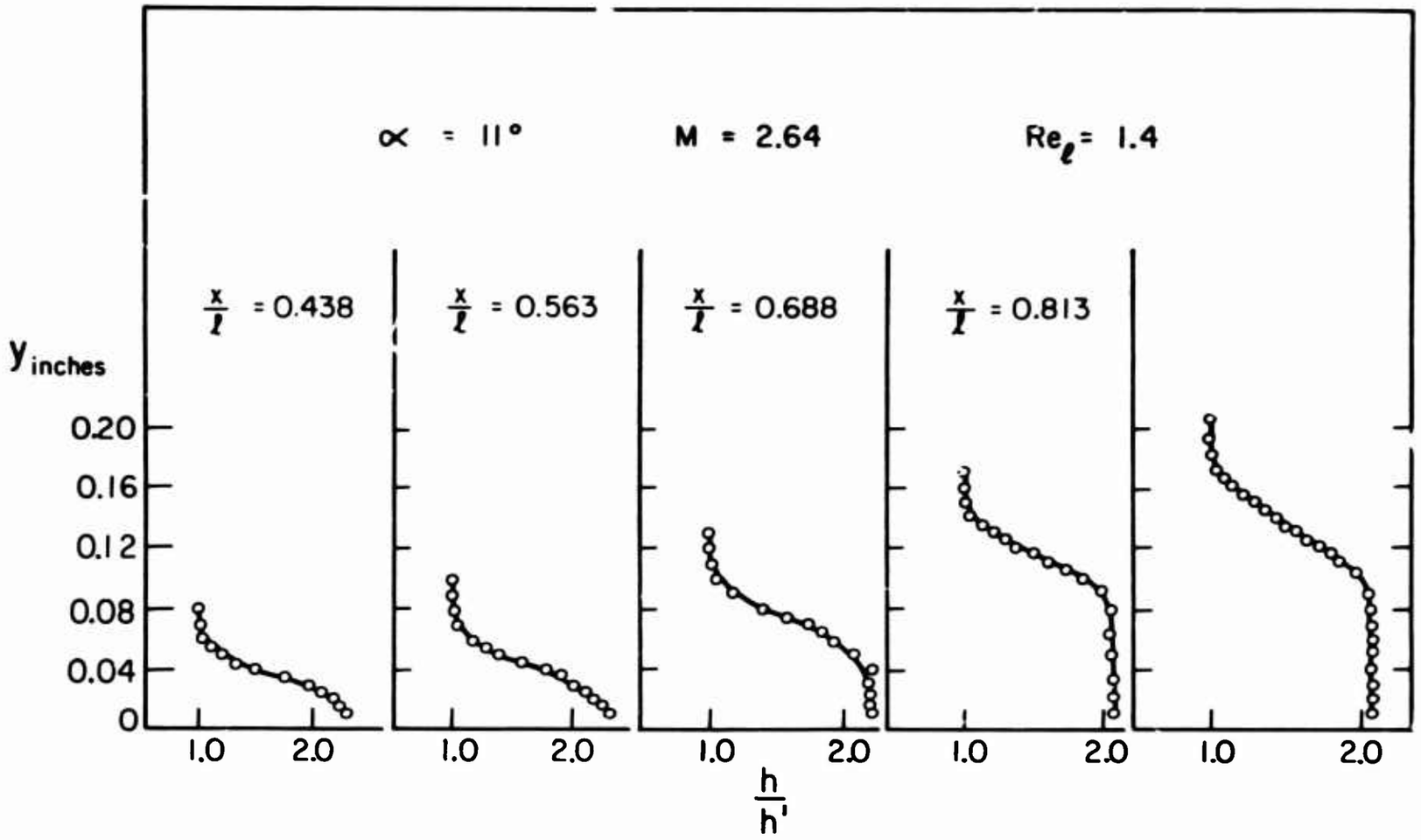


FIG. 16 STATIC ENTHALPY VARIATION AT DIFFERENT STATIONS AHEAD OF THE CORNER

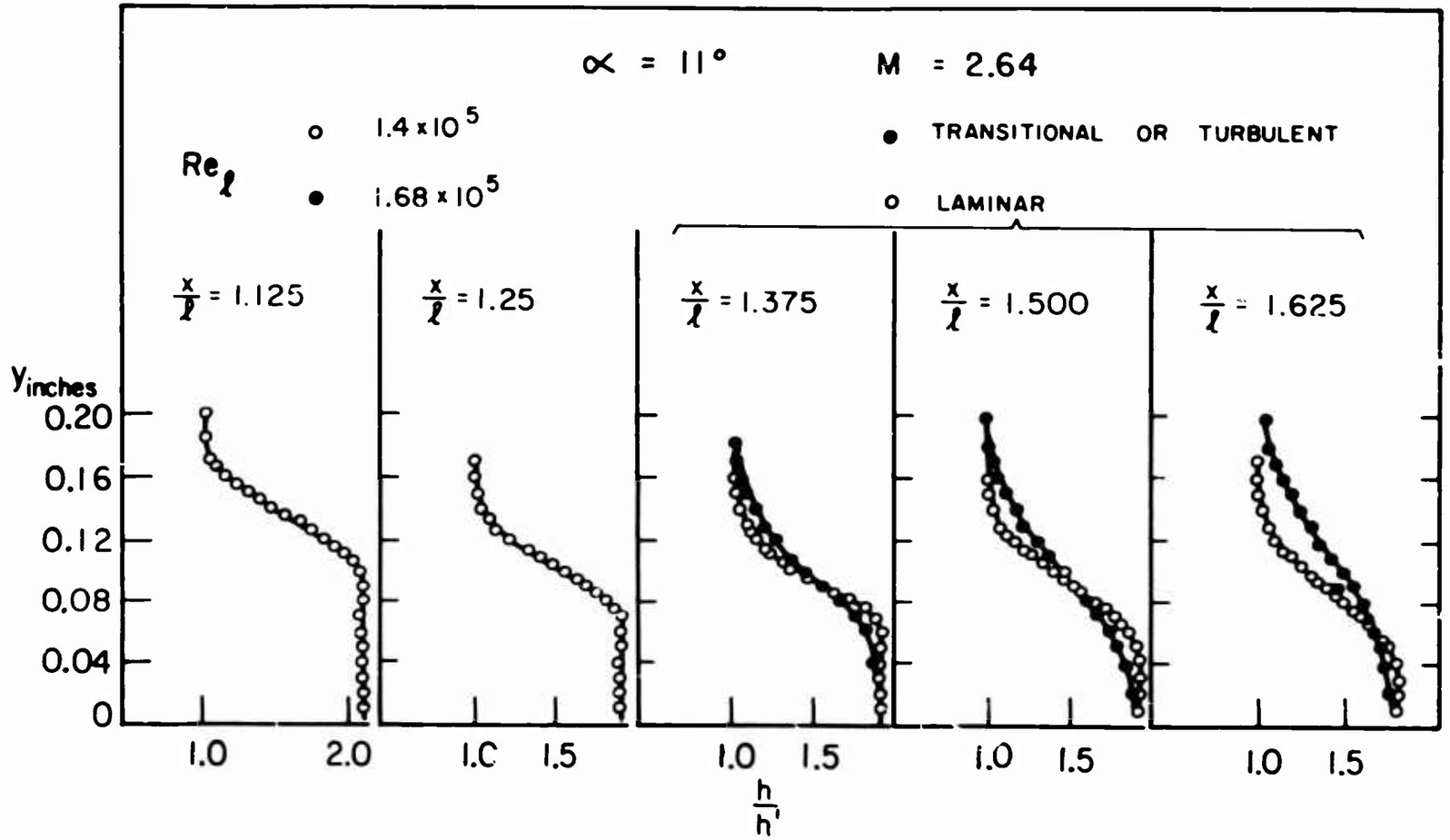


FIG. 17 STATIC ENTHALPY VARIATION AT DIFFERENT STATIONS DOWNSTREAM FROM THE CORNER

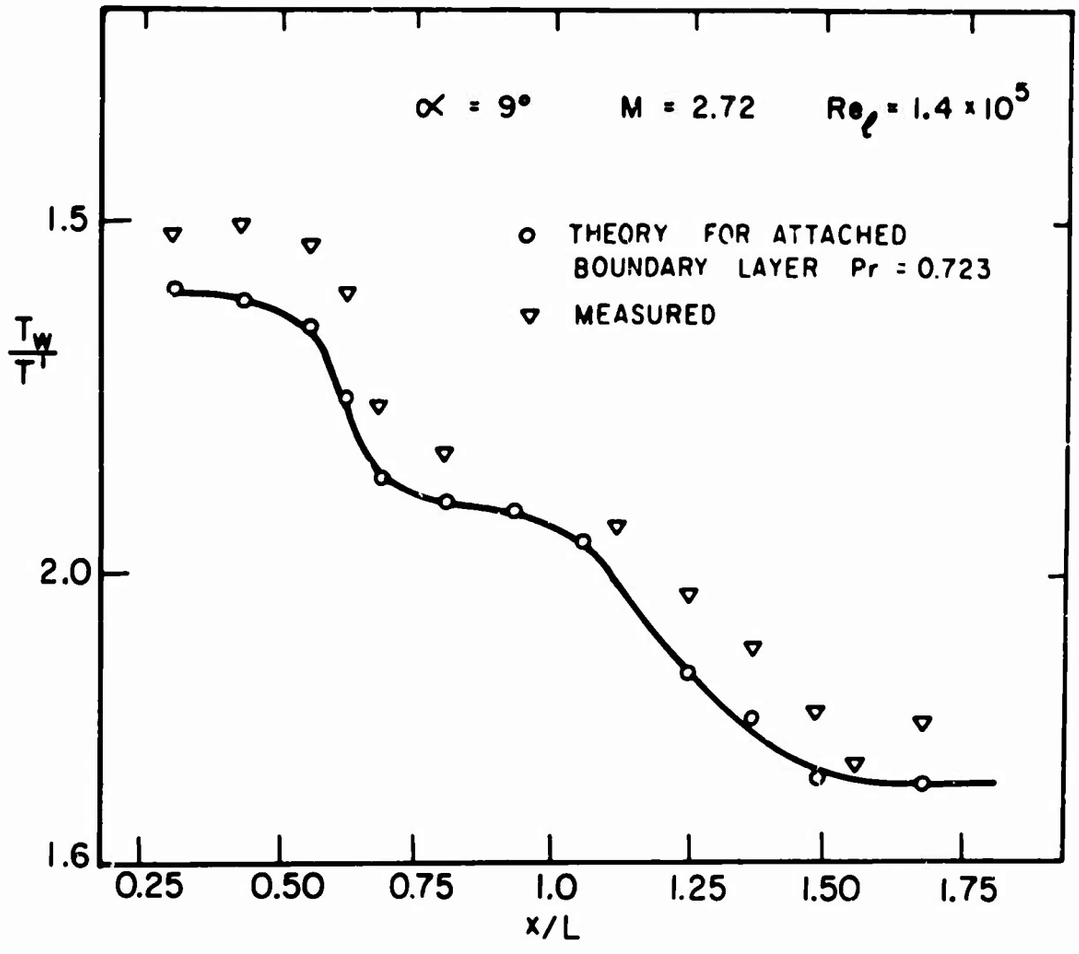


FIG. 18 COMPARISON OF $\frac{T_w}{T'}$ WITH THEORY

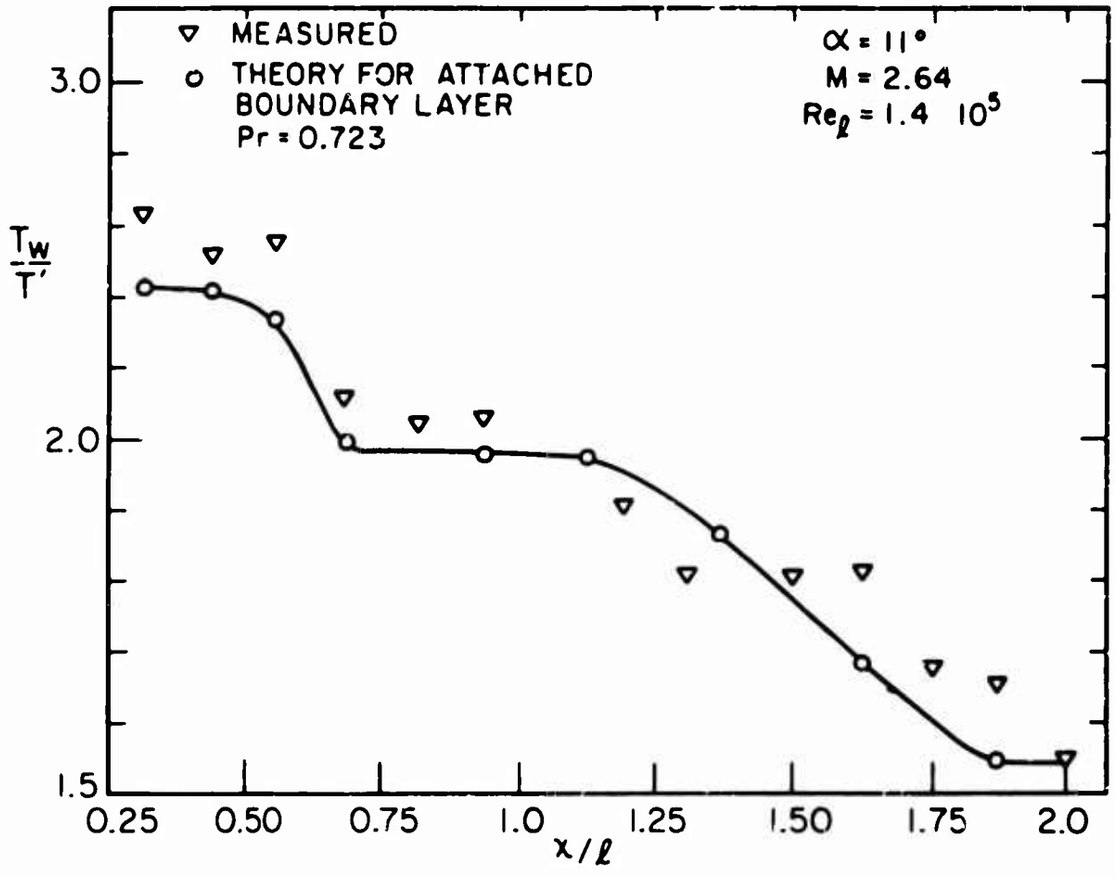


FIG. 19 COMPARISON OF $T_w/T'$ WITH THEORY

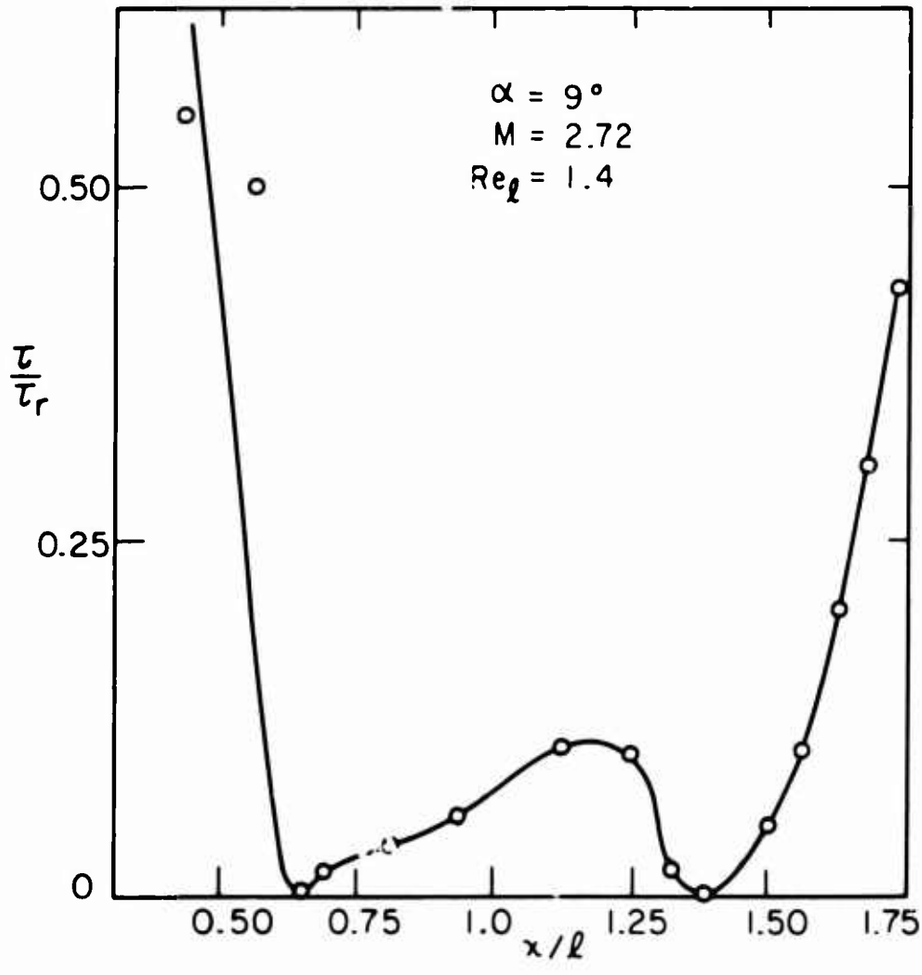


FIG. 20 SHEAR STRESS ALONG WALL AND u =0 LINE

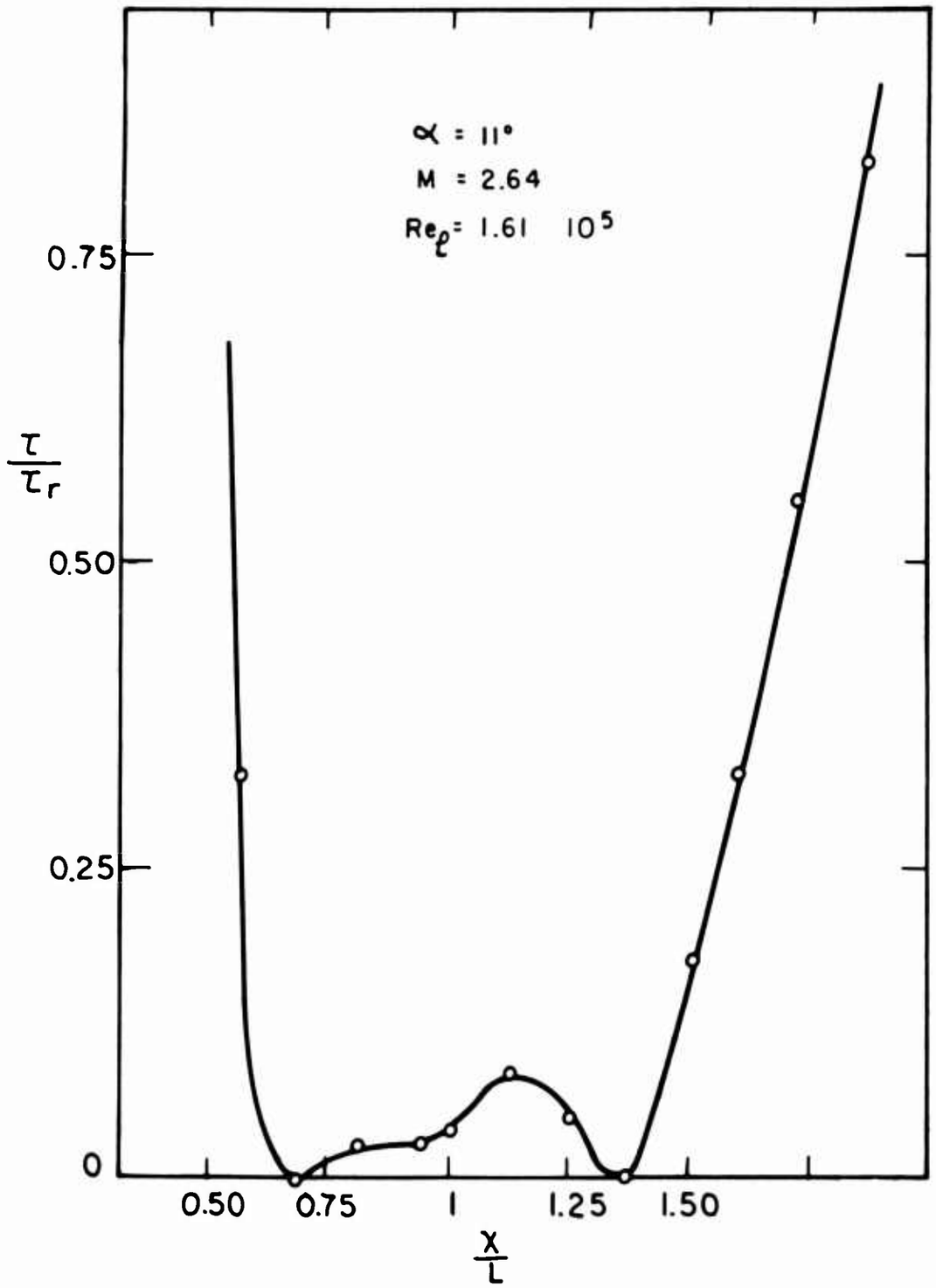


FIG. 21 SHEAR STRESS ALONG WALL AND u=0 LINE

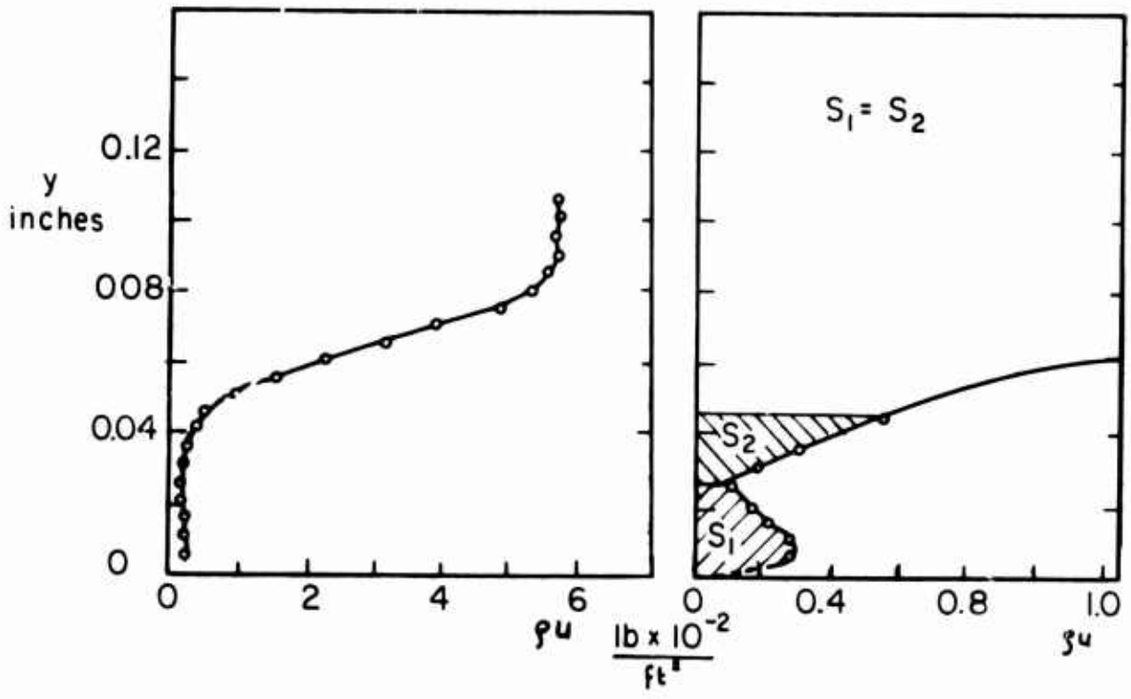


FIG. 22 GRAPHICAL DETERMINATION OF THE SEPARATING STREAMLINE

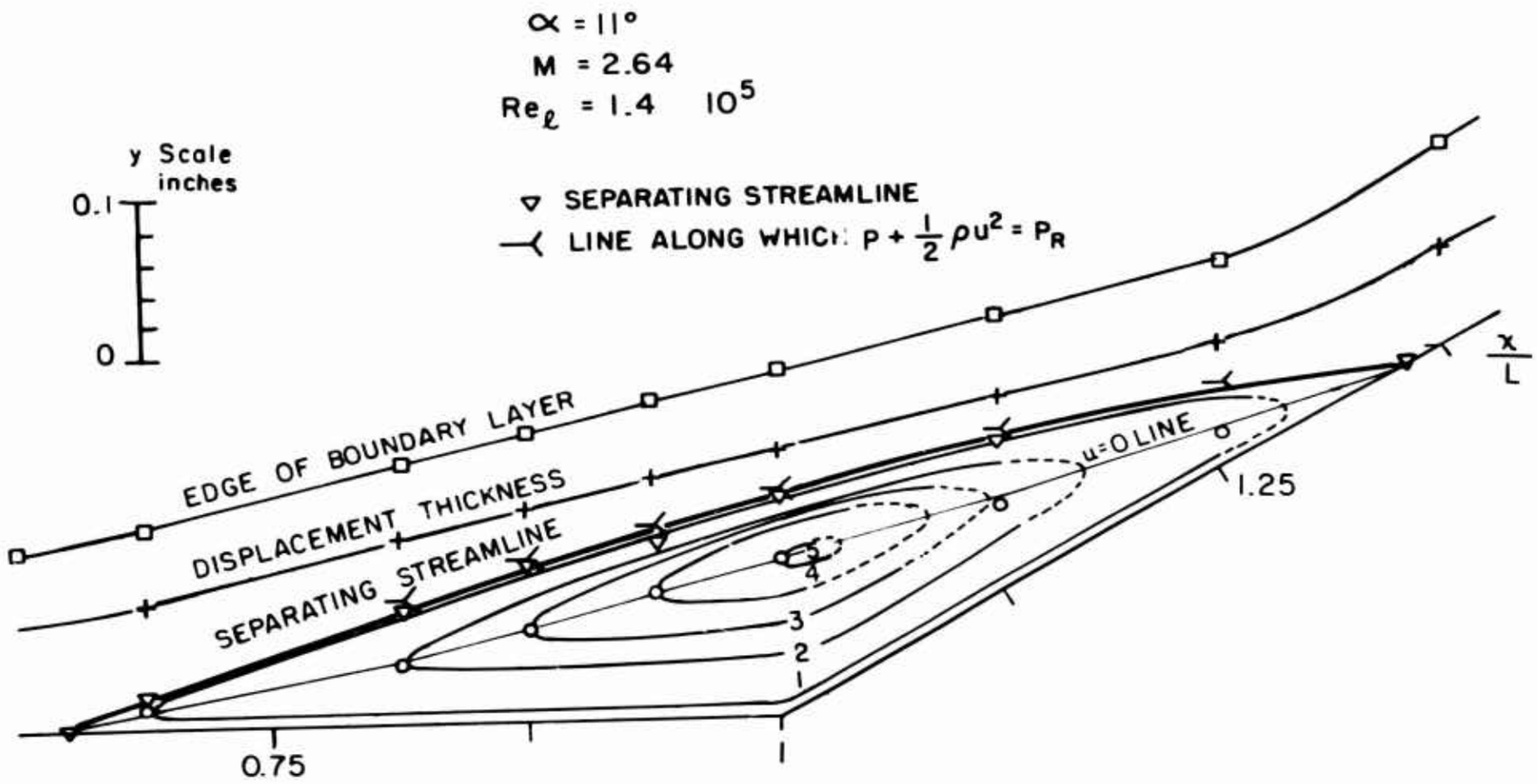


FIG. 23 DETAILS OF FLOW INSIDE THE SEPARATED BUBBLE

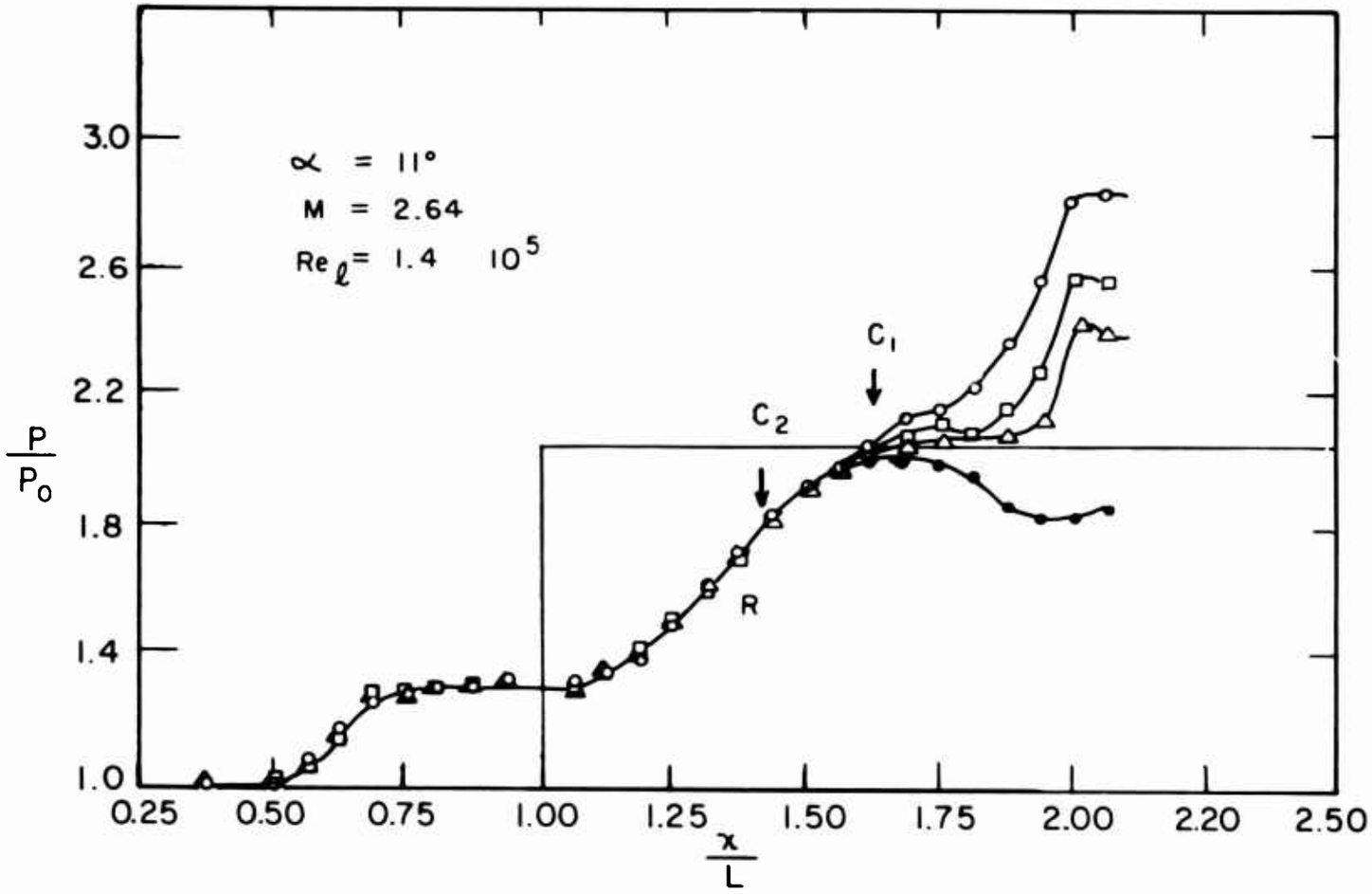


FIG.24 EFFECTS OF CHANGE IN THE DOWNSTREAM CONDITIONS - CRITICAL POINTS

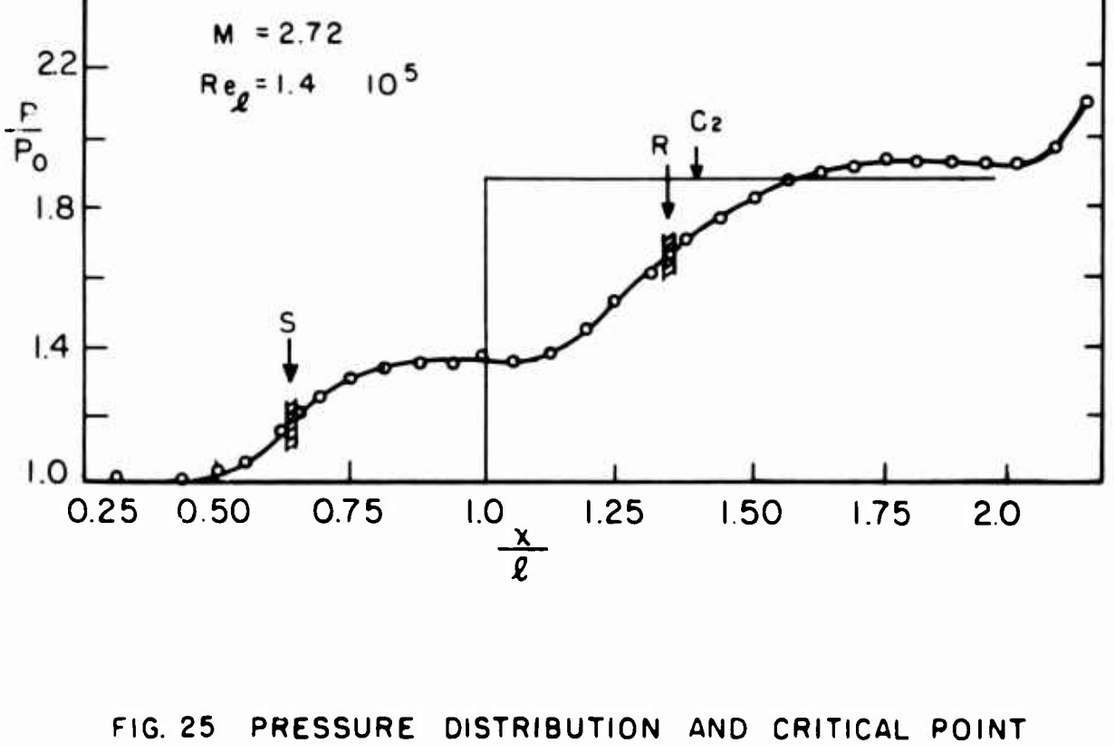


FIG. 25 PRESSURE DISTRIBUTION AND CRITICAL POINT

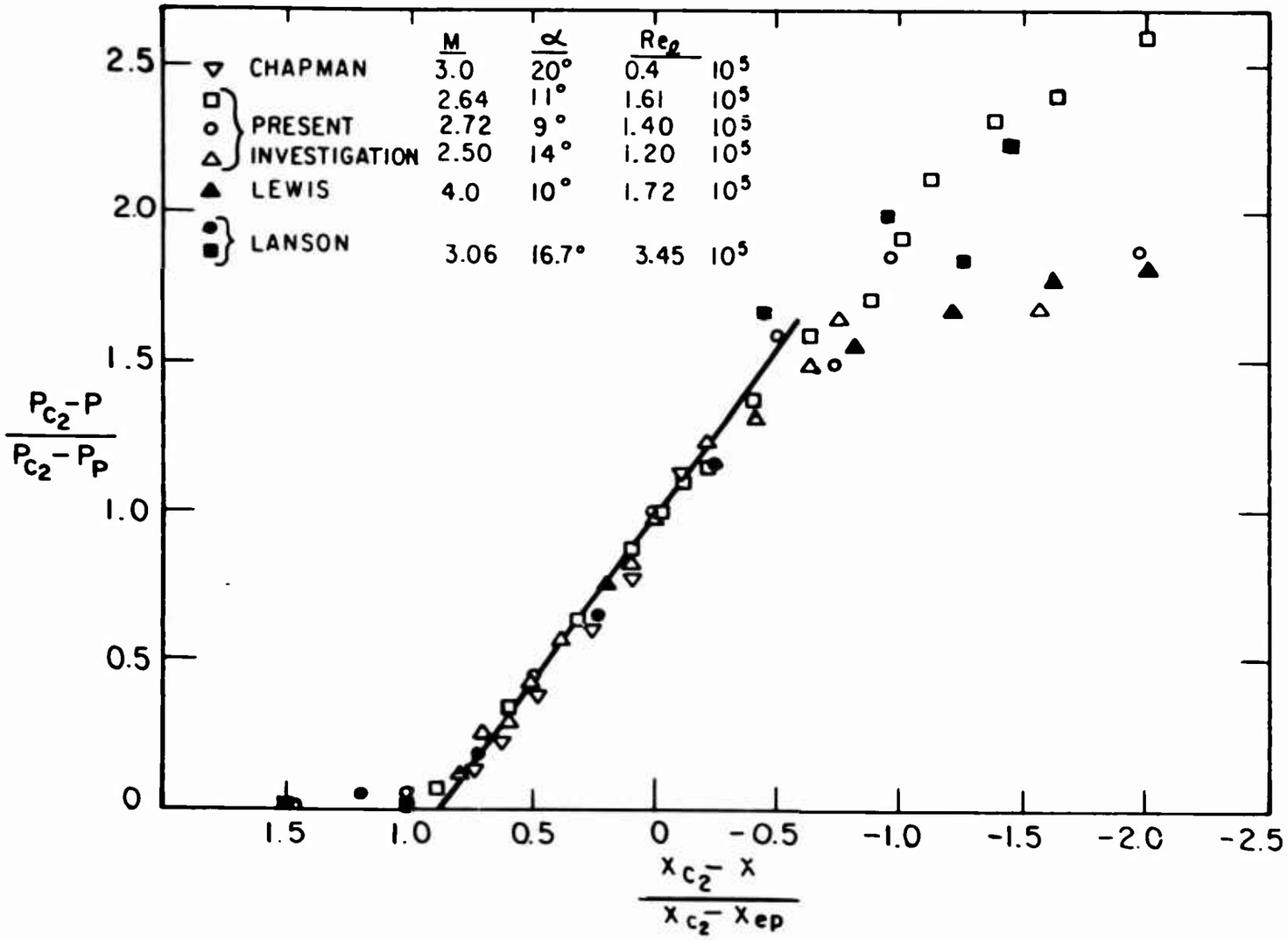


FIG.26 PROPERTY OF SECOND CRITICAL POINT

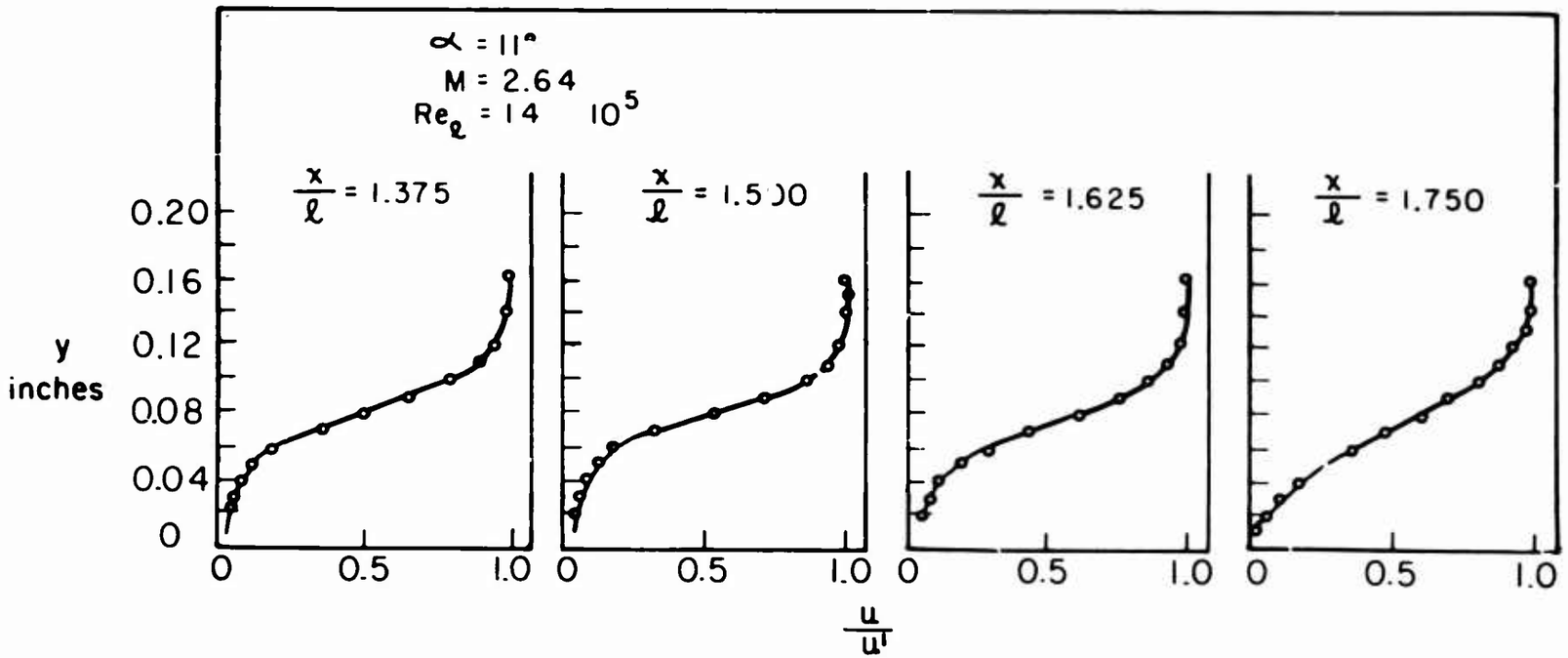


FIG.27 LAMINAR FLOW DOWNSTREAM OF REATTACHEMENT

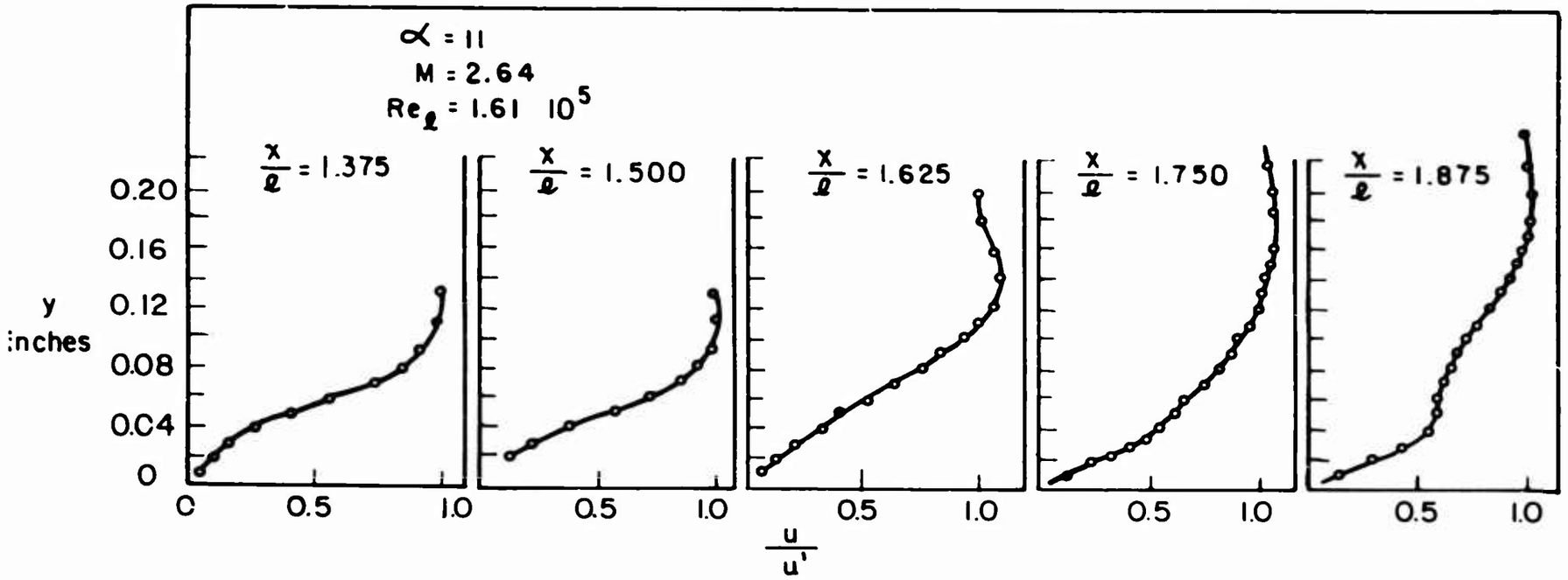


FIG. 28 TRANSITIONAL FLOW DOWNSTREAM OF REATTACHEMENT

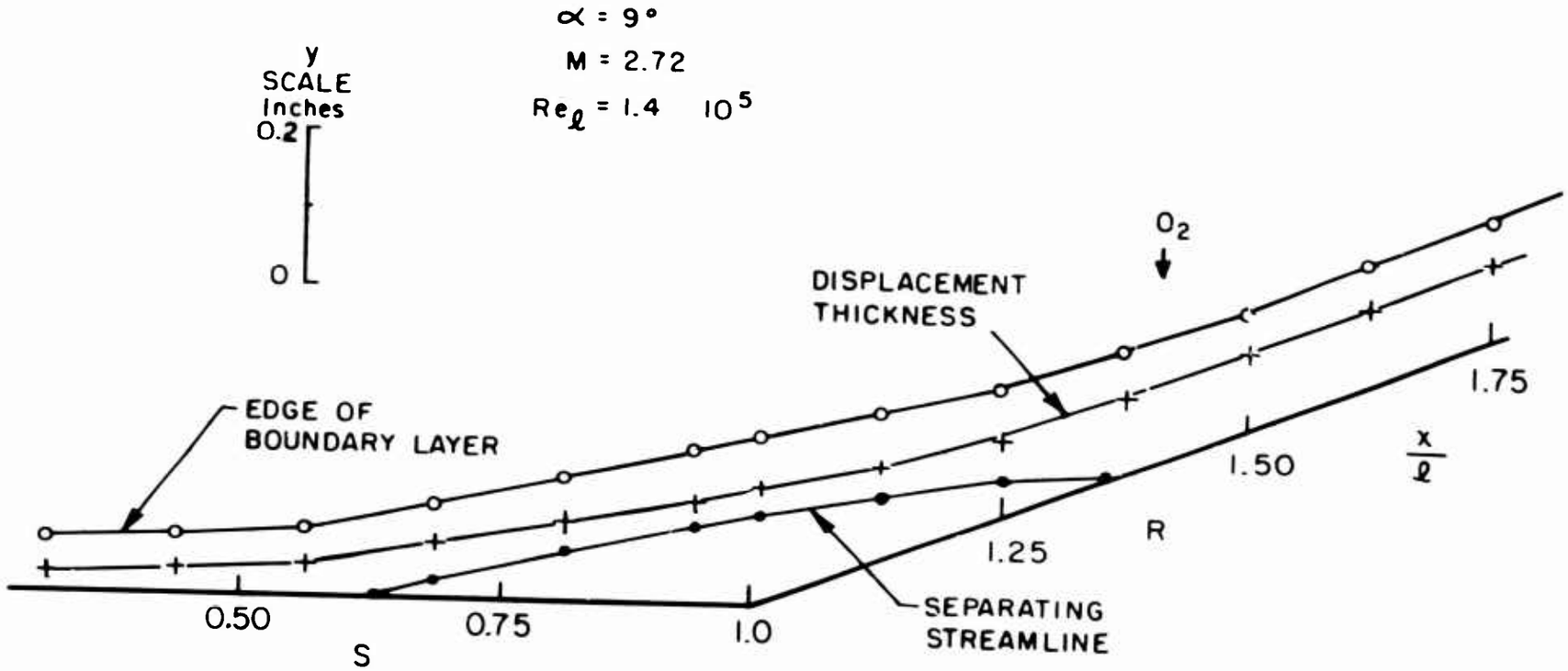


FIG. 29 FLOW FIELD FOR LAMINAR ATTACHEMENT

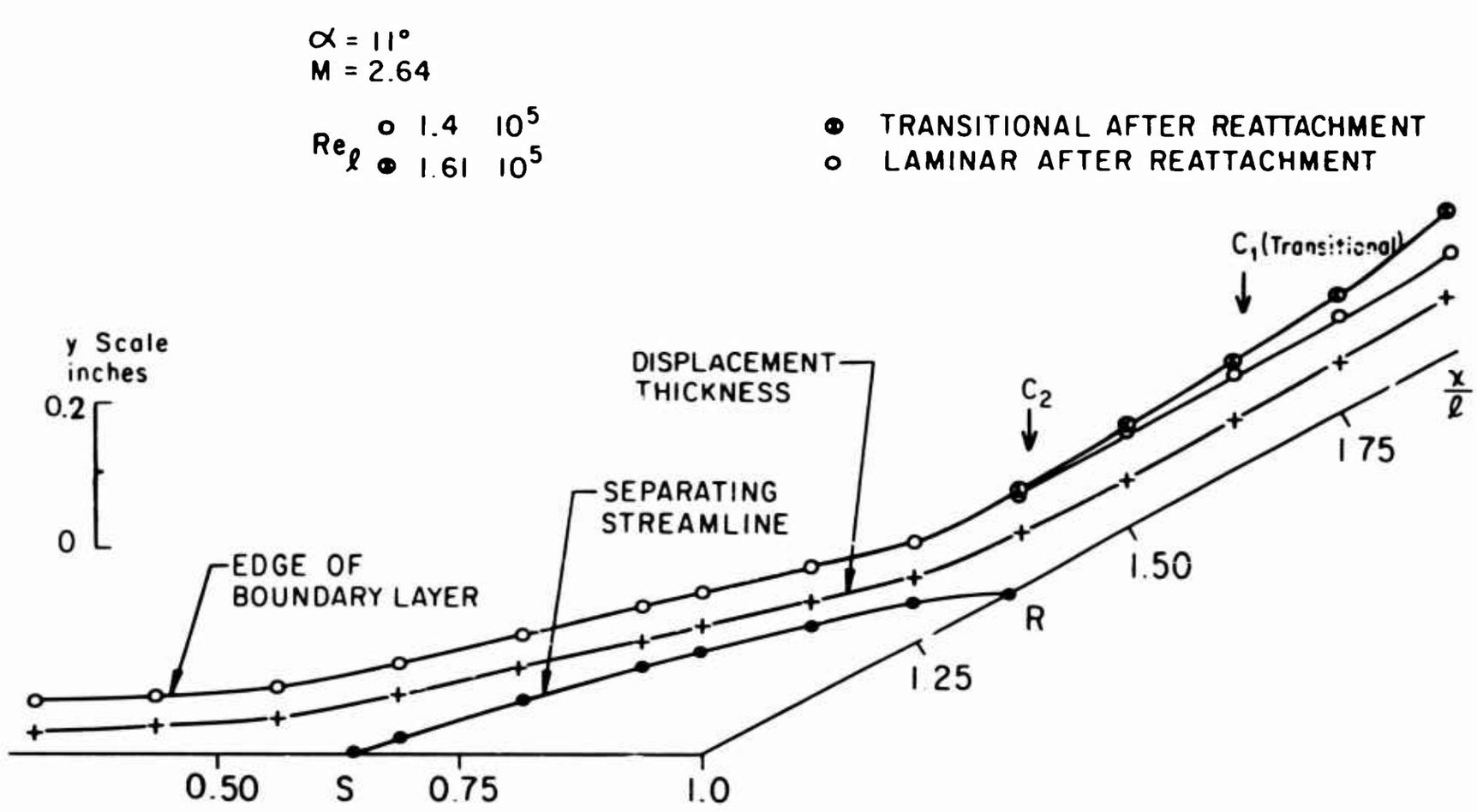


FIG. 30 FLOW FIELD FOR LAMINAR AND TRANSITIONAL REATTACHMENT

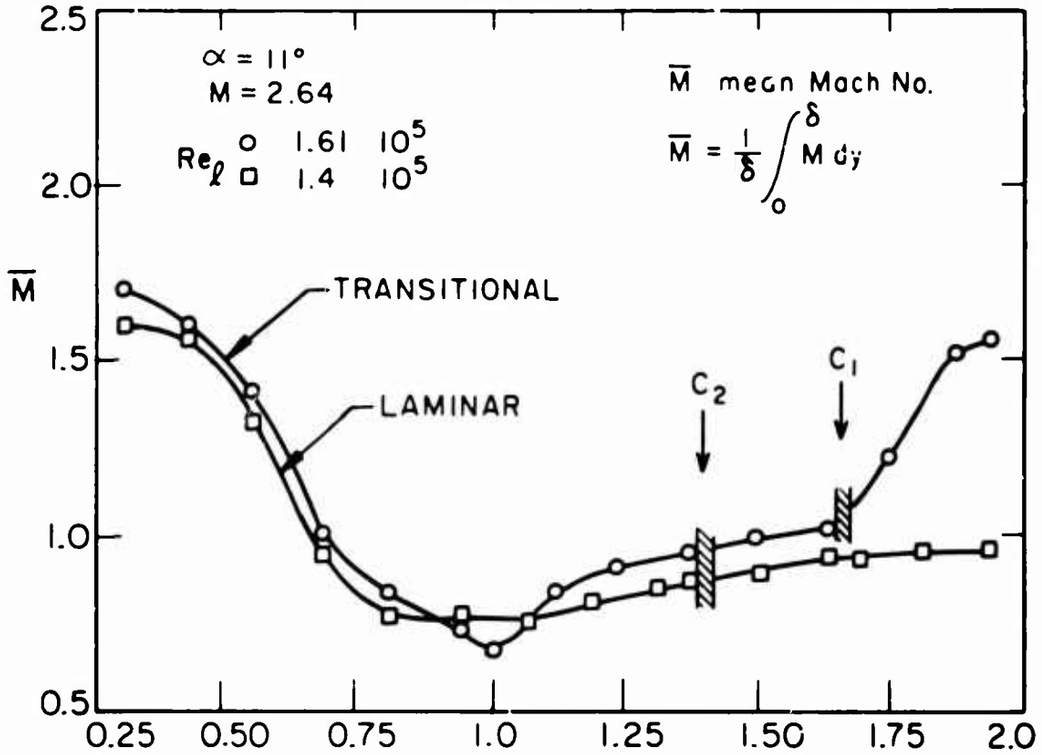


FIG. 31 VARIATION OF THE MEAN MACH NUMBER

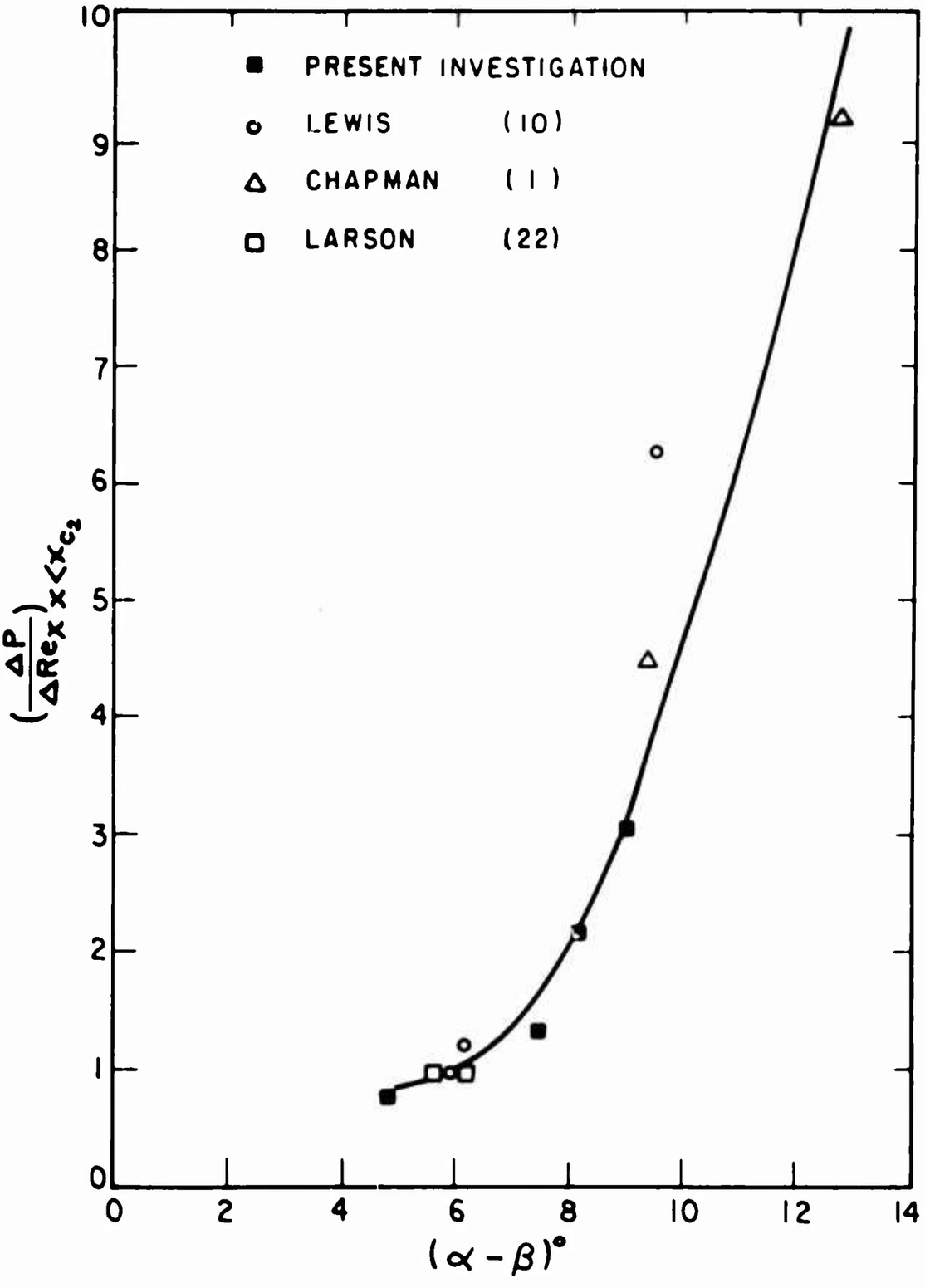


FIG. 32 VARIATION OF THE SLOPE OF THE PRESSURE DISTRIBUTION AHEAD OF THE CRITICAL POINT

# APPENDIX

## 1. End Losses Correction Factors

The Nusselt number end loss correction factor is given by:

$$C_N = \frac{\bar{a}_w}{a^*_w} \frac{1 + a^*_w}{1 + \bar{a}_w}$$

where $\bar{a}_w/a^*_w$ as a function of $S$ is represented in Fig. A-1.

The recovery temperature correction factor is given by

$$C_R = [1 - \omega ( \frac{\eta_S}{\eta_m} )] (1 - \omega)^{-1}$$

where $\omega/(1-\omega)$ as a function of $S$ is given in Fig. A-1.

A series of runs was made to determine the needle support temperature $T_S$. A resistance thermocouple (actually using a hot wire as a resistance thermocouple) was mounted on one needle and the temper- at different Mach numbers was measured. The results are shown in Fig. A-2, together with the predicted recovery temperature of cones in supersonic flow using laminar boundary layer theory. It is this predicted recovery temperature which was used in the computation of $\eta_S$. Although the predicted value is very close to the experimental one it is still thought that this procedure is far from perfect, mainly because the hot wire is soft soldered near the tip of the needle and it is this local temperature which should be used. For each series of runs the same wire was used, so that the error due to the support temperature appears systematically in all the data.

## 2. Heat Losses and Recovery Temperature as Functions of M, $Re_o$ and $Kn_\infty$

The empirical relation $Nu_o(Re_o,M)$ mentioned in Section 3.23 is of the form:

$$Nu_o(Re_o,M) = Nu_o(Re_o,\infty)\phi(Re_o,M)$$

where

$$Nu_o(Re_o,\infty) = Re_o^{\,n}[0.14 + N_1 + N_2] \quad ,$$

with:

$$n = 1 - \frac{Re_o^{\,0.6713}}{5.142 + 2\,Re_o^{\,0.6713}}$$

$$N_1 = \frac{0.2302\,Re_o^{\,0.7114}}{15.44 + Re_o^{\,0.7114}}$$

$$N_2 = \left(\frac{0.01569}{0.3077 + Re_o^{\,0.7378}}\right)\left(\frac{5}{15 + Re_o^{\,3}}\right)$$

and

$$\phi(Re_o,M) = 1 + \phi_1 \times \phi_2 \times \phi_3$$

with

$$\phi_1 = \frac{0.6039}{M} + 0.5701\left[\left(\frac{M^{1.222}}{1 + M^{1.222}}\right)^{1.569} - 1\right]$$

$$\phi_2 = 1.834 - 1.634\left(\frac{Re_o^{\,1.109}}{2.765 + Re_o^{\,1.109}}\right)$$

$$\phi_3 = 1 + \left(0.300 - \frac{0.065}{M^{1.67}}\right)\left(\frac{Re_o}{4 + Re_o}\right)$$

As stated in Section 3.2.3, the above relation is a curve fit for existing experimental results. This curve fit gives good accuracy

(±1%) for $M > 0.45$; below this value a more accurate curve fit is proposed (see (20))

$$\phi_3 = b_1 + c_1 \{1 - \exp[- a_1 ( Re_o - 6 )^{n_1} ( \frac{Re_o - 6}{Re_o - 6} )\}^2$$

where

$$b_1 = 0.05 + 2.9 \; M^{1.15}$$

$$c_1 = 0.05 + 3.08 \; M^{1.15}$$

$$e_1 = 0.6 + 1.25 \; M$$

$$n_1 = 1.137 \; \ell n \frac{\ell n[1 + \sqrt{\left| \frac{e_1 - b_1}{c_1} \right|} \; ]}{\ell n(1 + \sqrt{\left| \frac{e_1 - b_1}{c_1} \right|} \; ]} \; ;$$

$$a_1 = 0.1695^{n_1} \; \ell n[1 + \sqrt{\left| \frac{e_1 - b_1}{c_1} \right|} \; ]$$

This value has been used in our computation when $M < 0.45$.

The relations giving $\bar{\eta}_*$, $\eta_f$ and $\eta_c$ are the following:

$$\bar{\eta}_* = \frac{Kn_\infty^{1.193}}{0.4930 + Kn_\infty^{1.193}}$$

$$\eta_c = 1 - 0.05 \; ( \frac{M^{3.5}}{1.175 + M^{3.5}}$$

and

$$\eta_f - \eta_c = 0.2167 \; ( \frac{M^{2.8}}{0.8521 + M^{2.8}} )$$

As stated in Section 3.23, the relations $Nu_o(Re_o, M)$ could be transformed to $Nu_o(M, T_t, p)$ because we can write

$$Re_o = M \frac{dp}{\mu_t \sqrt{T_t}} \sqrt{\frac{\gamma}{R}} \left(1 + \frac{\gamma-1}{2} M^2\right)^{1/2}$$

and, substituting for $\gamma, R$ and using Sutherland's viscosity law, we get:

$$Re_o + M\, p \left(1 + \frac{M^2}{5}\right)^{1/2} \frac{21.015\, T_t + 4173.58}{T_t^2} \quad .$$

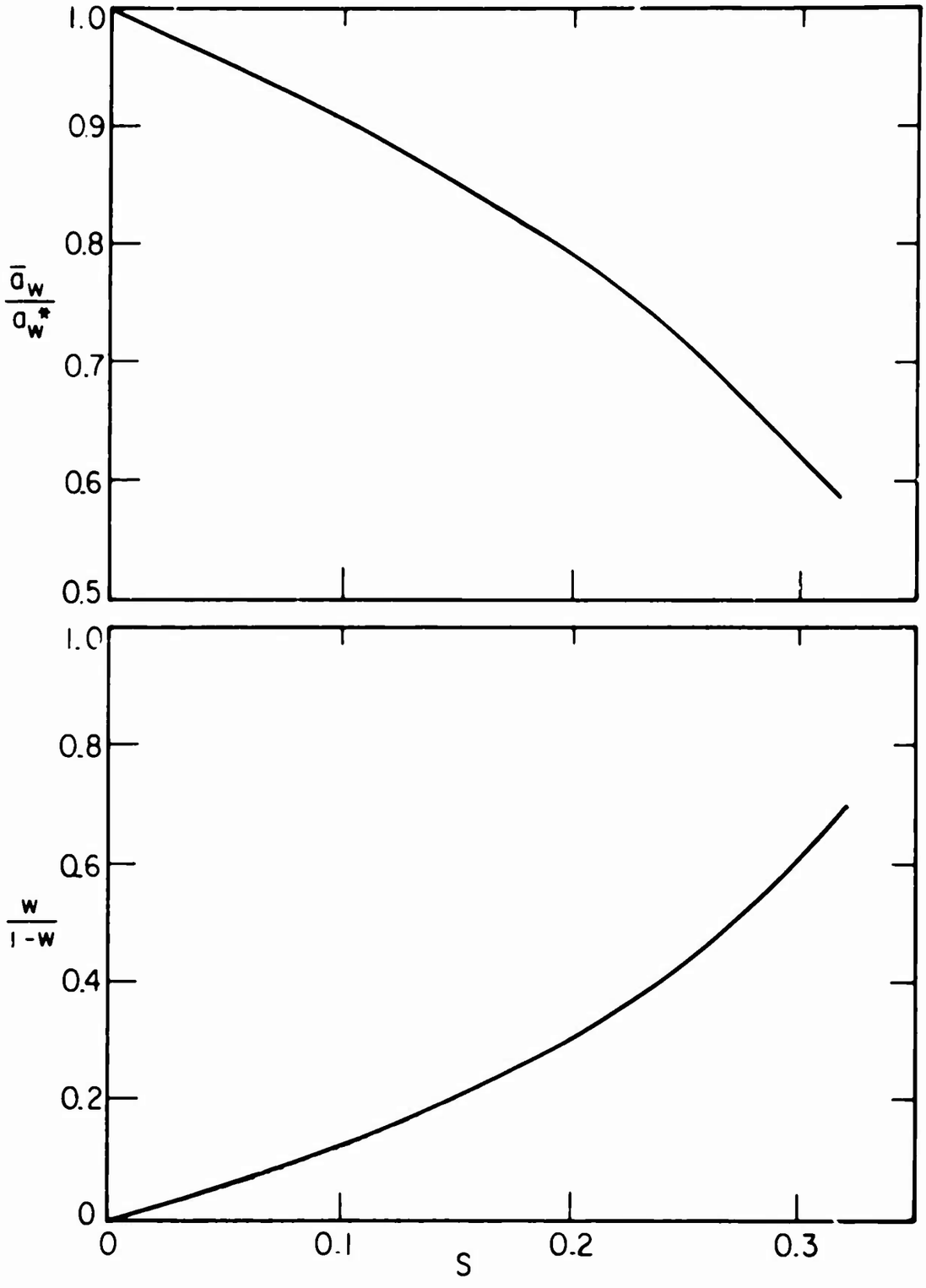


FIG. A-1 END LOSS CORRECTION FACTORS

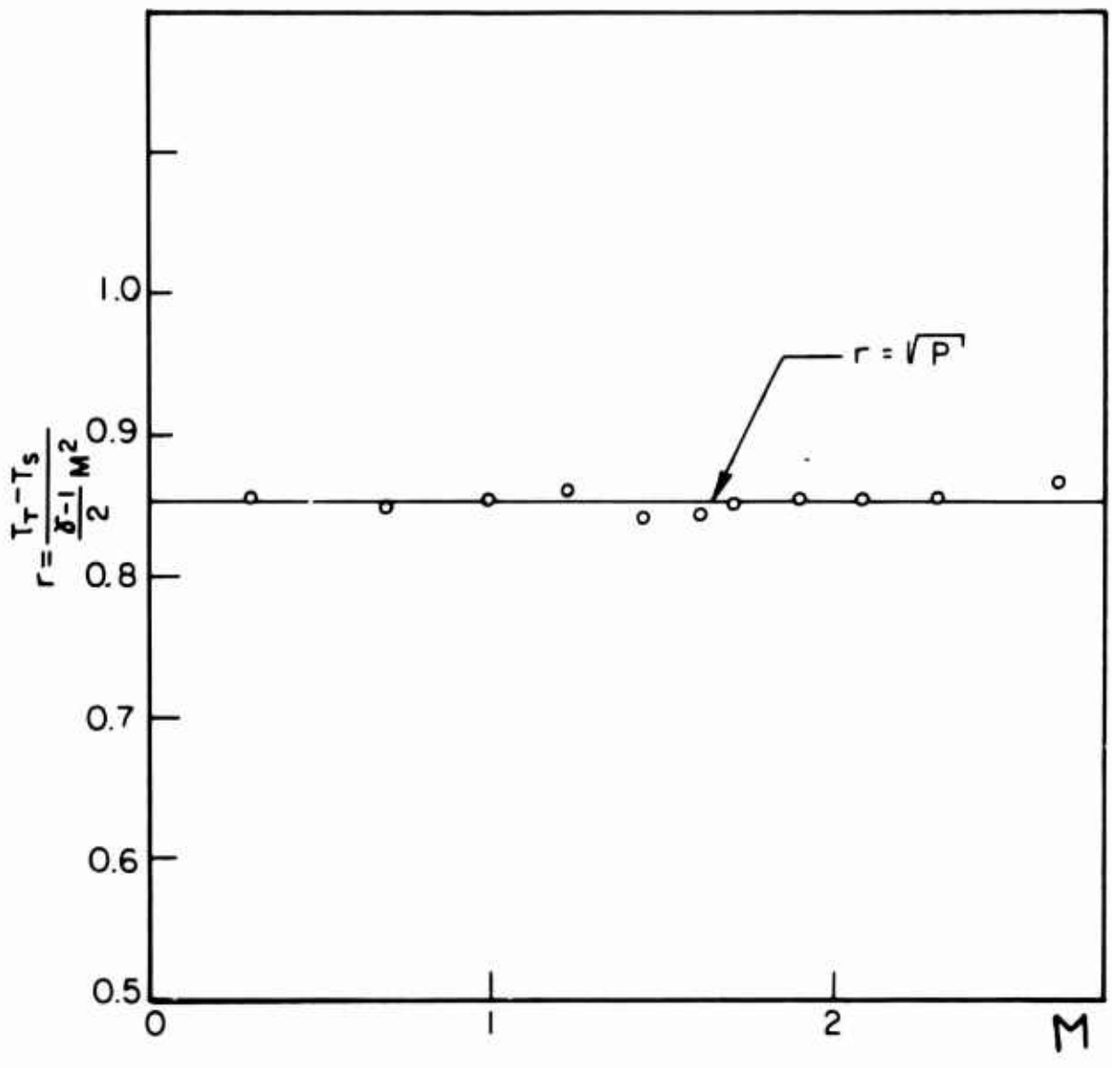


FIG. A-2 NEEDLE SUPPORT TEMPERATURE

Unclassified
Security Classification

**DOCUMENT CONTROL DATA - R&D**

*(Security classification of title, body of abstract and indexing annotation must be entered when the overall report is classified)*

| | |
|---|---|
| 1 ORIGINATING ACTIVITY (Corporate author)<br>Aeronautical Sciences Division<br>University of California, Berkeley | 2a REPORT SECURITY CLASSIFICATION<br>Unclassified<br>2b GROUP |

3 REPORT TITLE
Supersonic Laminar Boundary Layer Separation Near a Compression Corner

4 DESCRIPTIVE NOTES (Type of report and inclusive dates)
Technical Report

5 AUTHOR(S) (Last name, first name, initial)
A. A. Sfeir

| 6 REPORT DATE | 7a TOTAL NO OF PAGES | 7b NO OF REFS |
|---|---|---|
| March 1969 | 78 | 22 |

| | |
|---|---|
| 8a CONTRACT OR GRANT NO<br>AFOSR Grant 268-68 | 9a ORIGINATOR'S REPORT NUMBER(S)<br>AS-69-6 |
| b PROJECT NO | |
| c | 9b OTHER REPORT NO(S) (Any other numbers that may be assigned this report) |
| d | |

10 AVAILABILITY/LIMITATION NOTICES
Qualified requesters may obtain copies of this report from DDC.

| 11 SUPPLEMENTARY NOTES | 12 SPONSORING MILITARY ACTIVITY |
|---|---|
| | U.S. Air Force Office of Scientific Research |

13 ABSTRACT

Detailed measurements were performed in the region of interaction of a laminar boundary layer with a compression corner at Mach numbers near 2.5. Different models were tested permitting variation in the angle of compression and the conditions downstream of reattachment.

The heat flux and the resistance of equilibrium of a hot wire anemometer at any location in the flow field were measured. These measurements were supplemented by either the wall or the pitot pressure to compute all thermodynamic and dynamic variables.

The results permitted verification of the hypothesis of zero normal pressure gradients when the compression angle is small and the boundary layer is laminar. The enthalpy in the separated bubble was constant and equal to the wall enthalpy of a flat plate with attached laminar boundary layer at the same Mach number. Evidence of a reversed flow with velocities approximately 5% of the free stream velocity was observed. The recompression along the separating streamline was found to be very nearly isentropic. Critical points were located in the reattachment region and a physical explanation proposed with special emphasis on the location of transition.

DD FORM 1 JAN 64 1473

UNCLASSIFIED
Security Classification

UNCLASSIFIED

Security Classification

| 14. KEY WORDS | LINK A | | LINK B | | LINK C | |
|---|---|---|---|---|---|---|
| | ROLE | WT | ROLE | WT | ROLE | WT |
| Laminar supersonic boundary layer | | | | | | |
| Separated flow | | | | | | |
| Compression corner | | | | | | |
| Hot-wire measurements | | | | | | |
| Pitot measurements | | | | | | |
| Critical points | | | | | | |

## INSTRUCTIONS

1. **ORIGINATING ACTIVITY:** Enter the name and address of the contractor, subcontractor, grantee, Department of Defense activity or other organization *(corporate author)* issuing the report.

2a. **REPORT SECURITY CLASSIFICATION:** Enter the overall security classification of the report. Indicate whether "Restricted Data" is included. Marking is to be in accordance with appropriate security regulations.

2b. **GROUP:** Automatic downgrading is specified in DoD Directive 5200.10 and Armed Forces Industrial Manual. Enter the group number. Also, when applicable, show that optional markings have been used for Group 3 and Group 4 as authorized.

3. **REPORT TITLE:** Enter the complete report title in all capital letters. Titles in all cases should be unclassified. If a meaningful title cannot be selected without classification, show title classification in all capitals in parenthesis immediately following the title.

4. **DESCRIPTIVE NOTES:** If appropriate, enter the type of report, e.g., interim, progress, summary, annual, or final. Give the inclusive dates when a specific reporting period is covered.

5. **AUTHOR(S):** Enter the name(s) of author(s) as shown on or in the report. Enter last name, first name, middle initial. If military, show rank and branch of service. The name of the principal author is an absolute minimum requirement.

6. **REPORT DATE:** Enter the date of the report as day, month, year, or month, year. If more than one date appears on the report, use date of publication.

7a. **TOTAL NUMBER OF PAGES:** The total page count should follow normal pagination procedures, i.e., enter the number of pages containing information.

7b. **NUMBER OF REFERENCES:** Enter the total number of references cited in the report.

8a. **CONTRACT OR GRANT NUMBER:** If appropriate, enter the applicable number of the contract or grant under which the report was written.

8b, 8c, & 8d. **PROJECT NUMBER:** Enter the appropriate military department identification, such as project number, subproject number, system numbers, task number, etc.

9a. **ORIGINATOR'S REPORT NUMBER(S):** Enter the official report number by which the document will be identified and controlled by the originating activity. This number must be unique to this report.

9b. **OTHER REPORT NUMBER(S):** If the report has been assigned any other report numbers *(either by the originator or by the sponsor)*, also enter this number(s).

10. **AVAILABILITY/LIMITATION NOTICES:** Enter any limitations on further dissemination of the report, other than those imposed by security classification, using standard statements such as:

(1) "Qualified requesters may obtain copies of this report from DDC."

(2) "Foreign announcement and dissemination of this report by DDC is not authorized."

(3) "U. S. Government agencies may obtain copies of this report directly from DDC. Other qualified DDC users shall request through _____."

(4) "U. S. military agencies may obtain copies of this report directly from DDC. Other qualified users shall request through _____."

(5) "All distribution of this report is controlled. Qualified DDC users shall request through _____."

If the report has been furnished to the Office of Technical Services, Department of Commerce, for sale to the public, indicate this fact and enter the price, if known.

11. **SUPPLEMENTARY NOTES:** Use for additional explanatory notes.

12. **SPONSORING MILITARY ACTIVITY:** Enter the name of the departmental project office or laboratory sponsoring *(paying for)* the research and development. Include address.

13. **ABSTRACT:** Enter an abstract giving a brief and factual summary of the document indicative of the report, even though it may also appear elsewhere in the body of the technical report. If additional space is required, a continuation sheet shall be attached.

It is highly desirable that the abstract of classified reports be unclassified. Each paragraph of the abstract shall end with an indication of the military security classification of the information in the paragraph, represented as *(TS), (S), (C), or (U)*.

There is no limitation on the length of the abstract. However, the suggested length is from 150 to 225 words.

14. **KEY WORDS:** Key words are technically meaningful terms or short phrases that characterize a report and may be used as index entries for cataloging the report. Key words must be selected so that no security classification is required. Identifiers, such as equipment model designation, trade name, military project code name, geographic location, may be used as key words but will be followed by an indication of technical context. The assignment of links, roles, and weights is optional.

DD FORM 1 JAN 64 1473 (BACK)

UNCLASSIFIED

Security Classification